NASA/TM–2016-219338

Tuned Chamber Core Panel Acoustic Test Results

Noah H. Schiller and Albert R. Allen
Langley Research Center, Hampton, Virginia

September 2016

NASA STI Program . . . in Profile

Since its founding, NASA has been dedicated to the advancement of aeronautics and space science. The NASA scientific and technical information (STI) program plays a key part in helping NASA maintain this important role.

The NASA STI program operates under the auspices of the Agency Chief Information Officer. It collects, organizes, provides for archiving, and disseminates NASA's STI. The NASA STI program provides access to the NTRS Registered and its public interface, the NASA Technical Reports Server, thus providing one of the largest collections of aeronautical and space science STI in the world. Results are published in both non-NASA channels and by NASA in the NASA STI Report Series, which includes the following report types:

- TECHNICAL PUBLICATION. Reports of completed research or a major significant phase of research that present the results of NASA Programs and include extensive data or theoretical analysis. Includes compilations of significant scientific and technical data and information deemed to be of continuing reference value. NASA counter-part of peer-reviewed formal professional papers but has less stringent limitations on manuscript length and extent of graphic presentations.

- TECHNICAL MEMORANDUM. Scientific and technical findings that are preliminary or of specialized interest, e.g., quick release reports, working papers, and bibliographies that contain minimal annotation. Does not contain extensive analysis.

- CONTRACTOR REPORT. Scientific and technical findings by NASA-sponsored contractors and grantees.

- CONFERENCE PUBLICATION. Collected papers from scientific and technical conferences, symposia, seminars, or other meetings sponsored or co-sponsored by NASA.

- SPECIAL PUBLICATION. Scientific, technical, or historical information from NASA programs, projects, and missions, often concerned with subjects having substantial public interest.

- TECHNICAL TRANSLATION. English-language translations of foreign scientific and technical material pertinent to NASA's mission.

Specialized services also include organizing and publishing research results, distributing specialized research announcements and feeds, providing information desk and personal search support, and enabling data exchange services.

For more information about the NASA STI program, see the following:

- Access the NASA STI program home page at http://www.sti.nasa.gov

- E-mail your question to help@sti.nasa.gov

- Phone the NASA STI Information Desk at 757-864-9658

- Write to:
  NASA STI Information Desk
  Mail Stop 148
  NASA Langley Research Center
  Hampton, VA 23681-2199

NASA/TM–2016-219338

Tuned Chamber Core Panel Acoustic Test Results

Noah H. Schiller and Albert R. Allen
Langley Research Center, Hampton, Virginia

National Aeronautics and
Space Administration

Langley Research Center
Hampton, Virginia 23681-2199

September 2016

Acknowledgments

The authors gratefully acknowledge the contributions of Bart Zalewski and Joe Roche for their initial development of the tuned chamber core concept and for providing valuable technical insights during the evaluation. The testing would not have been possible without contributions from Anne McNelis, Bill Hughes, Bruce Rosenthal, and Dan Kosareo. Valuable guidance and support was provided throughout the project by Tom Krivanek, Cameron Cunningham, and Paul Senick. Finally, the contributions of Justin Jackson are acknowledged for his role in panel fabrication.

Available from:

NASA STI Program / Mail Stop 148
NASA Langley Research Center
Hampton, VA 23681-2199
Fax: 757-864-6500

Abstract

This report documents acoustic testing of tuned chamber core panels, which can be used to supplement the low-frequency performance of conventional acoustic treatment. The tuned chamber core concept incorporates low-frequency noise control directly within the primary structure and is applicable to sandwich constructions with a directional core, including corrugated-, truss-, and fluted-core designs. These types of sandwich structures have long, hollow channels (or chambers) in the core. By adding small holes through one of the facesheets, the hollow chambers can be utilized as an array of low-frequency acoustic resonators. These resonators can then be used to attenuate low-frequency noise (below 400 Hz) inside a vehicle compartment without increasing the weight or size of the structure.

The results of this test program demonstrate that the tuned chamber core concept is effective when used in isolation or combined with acoustic foam treatments. Specifically, an array of acoustic resonators integrated within the core of the panels was shown to improve both the low-frequency absorption and transmission loss of the structure in targeted one-third octave bands. For instance, with resonators tuned to 200 Hz, the measured Sabine absorption coefficient for the panel with integrated resonators was significantly increased, and the transmission loss of the structure was 5 dB larger than it was for the same panel without resonators. When the resonator tunings were spread over multiple one-third octave bands, the benefit was spread over those same one-third octave bands. These benefits were achieved with no change in the size or weight of the structure. Results also show that combining acoustic foam with tuned chamber core panels can result in better performance than either technology can provide alone. While the transmission loss benefit is additive, the interaction between the resonator array and the foam results in better low-frequency absorption than a simple linear combination would suggest. Furthermore, models are able to capture many of the trends observed during the tests. The promising results seen during this test series provide further motivation to test larger, and more realistic structures in the future.

Introduction

High interior noise levels in aerospace vehicles can damage sensitive equipment, affect passenger and crew health, and even impact vehicle acceptability. While high-frequency noise can often be mitigated with porous treatments, such as fiberglass and foam, low-frequency noise is more difficult to control without thick, heavy treatment. Acoustic resonators can help, but conventional resonator systems take up space and add weight to the vehicle. Minimizing these two parameters is critical, particularly in aerospace applications. Therefore, this report focuses on an alternative design that uses acoustic resonators integrated within the primary structure to attenuate low-frequency noise without reducing the usable interior space or increasing the overall weight of the vehicle. This design is referred to as a tuned chamber core (TCC) structure.

A tuned chamber core structure can be created using a variety of sandwich constructions, including corrugated-, truss-, and fluted-core designs. These types of directional sandwich structures have a high uniaxial bending stiffness and low mass, making them attractive alternatives for launch vehicle and aircraft applications. In addition, these structures have long hollow channels in the core that can be utilized as an array of low-frequency acoustic resonators. The resonators can be created by inserting light-weight partitions into the core to divide the channels into multiple chambers. Small holes can then be drilled through the inner facesheet and into each chamber. The holes function as the inlets to the acoustic resonators. An example of a tuned chamber core panel is shown in Figure 1. Since the natural frequency of the acoustic resonators can be tuned by varying the length of individual chambers, the concept enables targeted, low-frequency noise control without increasing the weight or size of the structure.

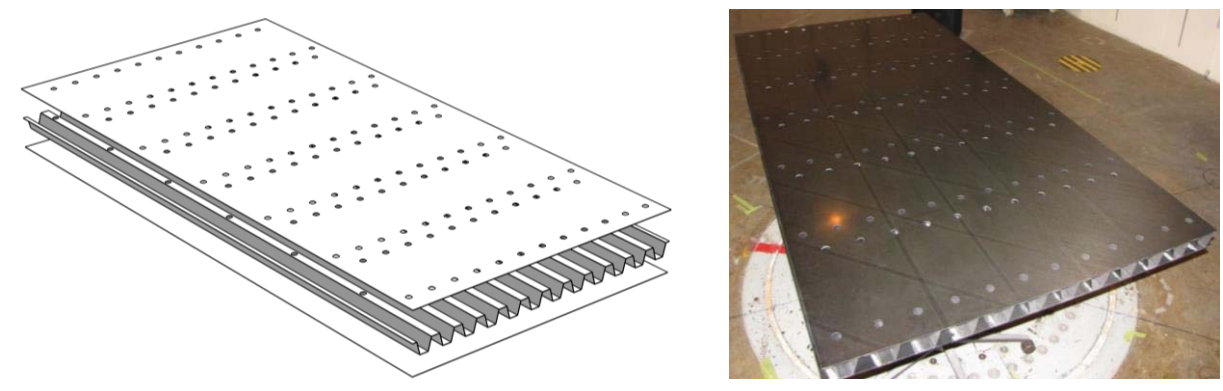

Figure 1: Tuned chamber core panel with inlets facing up: expanded view (left) and photograph (right) of a 4' by 8' TCC panel.

Researchers from the Air Force Research Laboratory and the University of Pittsburg have studied similar sandwich structures that contained acoustic resonators integrated within the primary structure [1,2]. They built and tested double-wall cylinders with long rectangular chambers sandwiched between inner and outer facesheets. Ports were added to the inner facesheet to couple the resonators to the interior volume. They demonstrated that the noise reduction, or difference between the average sound pressure outside and inside the cylinder, could be increased at targeted frequencies. Based on their promising results, similar corrugated sandwich panels containing acoustic resonators have been investigated at NASA [3,4]. For instance, sound transmission loss and absorption tests have been performed using lightweight, prototype panels. These tests were designed to characterize the low frequency performance of the concept and validate models that could eventually be used to generate vehicle level predictions. The results from the first round of tests were mixed [4], motivating the need for a second round of testing using more structurally representative panels.

This report documents the second round of acoustic testing performed on TCC panels and the subsequent model correlation activity. The goal of the tests was to collect data that could be used to validate vibroacoustic models of representative TCC structures and to evaluate combined configurations consisting of acoustic foam over TCC panels. The combined dataset was used to determine if the interaction between the low-frequency acoustic resonators and conventional foam treatment would be beneficial or detrimental to the overall performance of the system. This report begins with a description of the test articles. The facility and measurement procedures are then described followed by a brief overview of the modeling approach. A comparison of predictions and panel-level measurements are then presented and finally, some concluding remarks are provided.

Test Articles

This section describes the panels and foam material used during the test. While the primary objective of the test was to evaluate the performance of TCC panels, mass-loaded vinyl and honeycomb panels were also tested for comparison purposes. Therefore, descriptions of each type of panel are included as well as a description of the melamine foam used during the combined TCC and foam tests.

TCC Panels

The TCC panels are composite sandwich panels with a corrugated core, as shown in Figure 1. Three panels with nominally identical construction were built and tested: a 4' by 8' panel and two 4' by 4' panels. The panels have a nominal thickness of 2.2", which includes 0.063"-thick

facesheets over a 2.1”-tall corrugated core. The facesheets were fabricated from 8 plies of carbon-fiber fabric while the corrugated core consists of 2 fabric plies with a nominal thickness of 0.016”. During fabrication, the facesheets and core were pre-cured and then post-bonded with Hysol EA 9394 epoxy paste adhesive. This manufacturing approach resulted in an inconsistent bond between the facesheets and core that could be improved in subsequent builds. However despite this issue, the test articles were still adequate to meet the objectives of the acoustic test. The measured dimensions of the panels are slightly different than the nominal values, and are therefore included in Appendix A within Table 4. Additional details concerning the core geometry and layup are also included in Appendix A.

As shown in Figure 1, holes (0.875” diameter) were drilled in the top facesheet to function as the inlets to the acoustic resonators. The inlet locations for this test were selected to maximize the number of 200 Hz resonators that could be integrated into the panels. A target frequency of 200 Hz was selected based on the low frequency limitations associated with the test facility. As shown in Figure 2, the 4’ by 8’ panel contains 138 inlets arranged in 12 rows. Similarly, the 4’ by 4’ panels each contain 69 inlets arranged in 6 rows. Since each inlet is used for one acoustic resonator, the 4’ by 8’ panel contains 138 acoustic resonators and the 4’ by 4’ panels each contain 69 acoustic resonators.

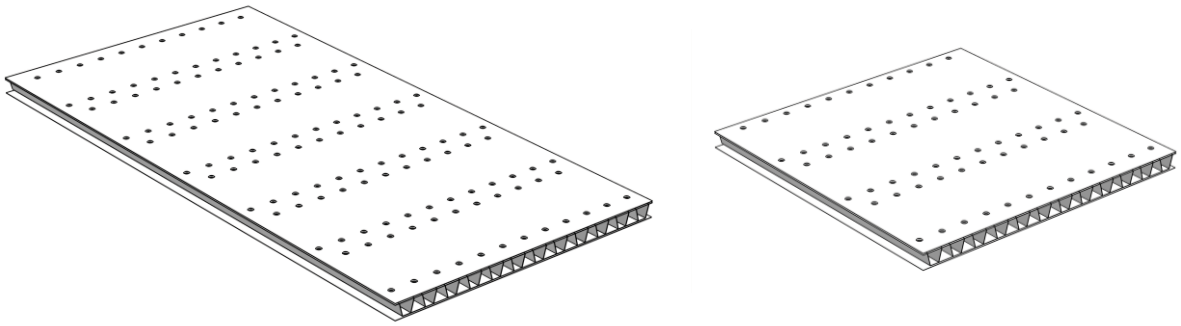

Figure 2: Location of inlet holes in the 4’ by 8’ panel (left) and 4’ by 4’ panel (right).

The corrugated core separating the two facesheets produced long channels that ran the entire length of the panels, which were either 8’ or 4’ long. However, all panels had the same nominal width (4’ in this case), so they all contained 23 channels. Before testing, light-weight foam plugs were used to partition each of the 23 channels into multiple chambers that could be used as acoustic resonators. Each chamber was sealed using two light-weight expanded polyethylene foam plugs that were inserted into the channels from the end of the panel and then slid into position. While foam plugs would probably not be used in the final application, they were used in this test series because they were easy to work with and allowed the acoustic resonators to be retuned. The foam plugs were nominally 1”-thick, and were die cut by the manufacturer into a trapezoidal shape, as shown in Figure 3, that was slightly larger than the channels within the core of the panels. Therefore, the plugs had to be compressed (slightly) as they were inserted into the core. This was meant to improve the seal around the perimeter of the plugs. However, the irregular bead of adhesive used to attach the core to the facesheet, shown in Figure 3, still resulted in small gaps around the perimeter of some foam plugs. Although the gaps were undesirable, they were expected to have little impact on the overall acoustic performance of the panels. The density of the expanded polyethylene foam is 1.3 lb/ft^3, and the weight of each plug was approximately 0.051 oz. Therefore, the 276 plugs used to seal the 138 chambers in the 4’ by 8’ panel weighed approximately 0.88 lb. Similarly, the 138 plugs used to seal the 69 acoustic resonators in the 4’ by 4’ panel weighed 0.44 lb. In comparison, the weight of the 4’ by 8’ panel (with plugs) was 49.0 lb, and the weight of each 4’ by 4’ panel was 25.8 lb. Therefore, the plugs accounted for less than 2% of the total panel mass.

Figure 3: Expanded polyethylene foam plug (left) and close-up of the core showing the extra adhesive (right).

The length of the chambers determined the natural frequency of the acoustic resonators, and this could be controlled by adjusting the position of the foam plugs. Two different tunings were considered during the test series. In one configuration, all of the resonators were tuned for approximately 200 Hz. This was achieved by positioning the plugs so that all the chambers had a length of approximately 11" with a single inlet near the end of the resonator, as depicted in Figure 4. In the 200 Hz configuration, 69% of the core volume was being used to create the array of acoustic resonators. A layout optimization procedure might be implemented to further improve volume utilization (and therefore performance) in future applications.

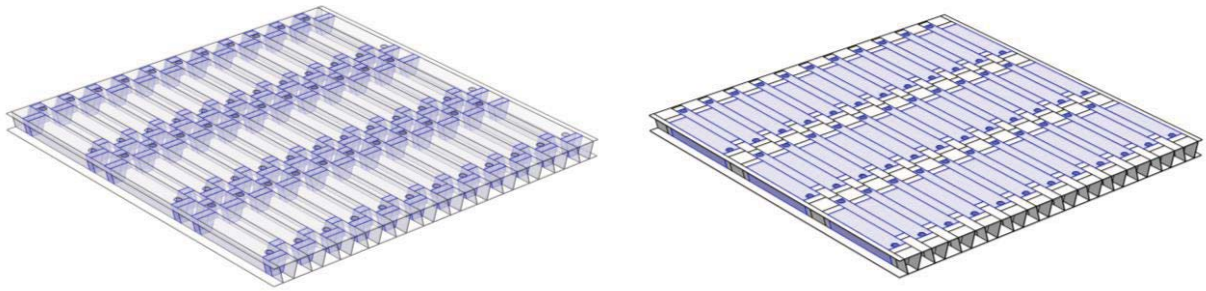

Figure 4: Plug positions used in the 200 Hz configuration (left) and spatial extent of the acoustic resonators (right), as illustrated for the 4' x 4' panel.

A second configuration with three different chamber lengths was also tested. Specifically, chamber lengths of 11", 7.5", and 5.5" were used to target 200 Hz, 250 Hz, and 315 Hz, respectively. Approximately 35% of the resonators were tuned for 200 Hz, 35% were tuned for 250 Hz, and 30% were tuned for 315 Hz. The corresponding location of the plugs in the 4' by 4' panel are shown in Figure 5 as an example. In this arrangement, 51% of the core volume was used in the array of acoustic resonators.

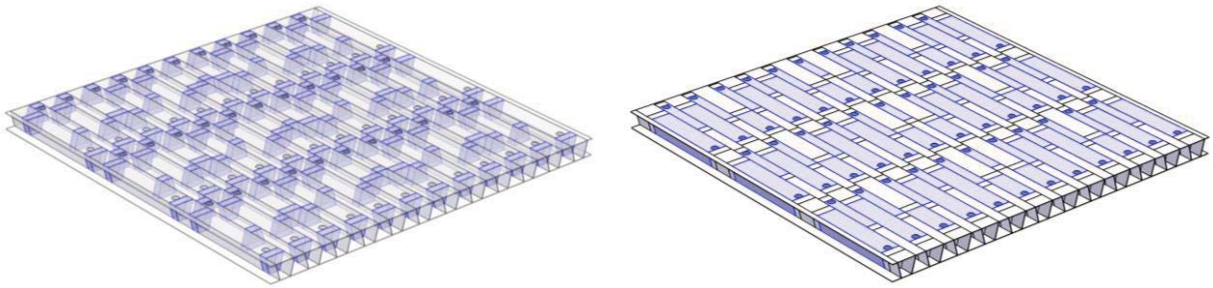

Figure 5: Plug positions used in the spread (200-315 Hz) configuration (left) and spatial extent of the acoustic resonators (right), as illustrated for the 4' x 4' panel.

Mass-Loaded Vinyl

Mass-loaded vinyl is used as a standard test article in many acoustical test facilities. Since the material is limp, the boundary conditions have little effect on the measured transmission loss. Therefore, repeat tests tend to give very similar results. This makes mass-loaded vinyl useful for quality control purposes since changes in the results can be indicative of problems with transducers, cabling, flanking paths, etc. The material is also very easy to model since it can be characterized by its size and mass per unit area. Therefore, measurements and predictions can be compared to provide a check on the test setup. The mass-loaded vinyl used during this test series was 0.1" thick with a mass per unit area of 1.00 lb/ft^2 and is shown in Figure 6. Two sizes were tested, a 4' by 8' sample and a 4' by 4' sample.

Figure 6: Mass-loaded vinyl.

Honeycomb Panels

The honeycomb sandwich panel is depicted in Figure 7. Once again, three panels with nominally identical construction were built, a 4' by 8' panel, and two 4' by 4' panels. The panels have a nominal thickness of 1.12", which includes 0.048"-thick facesheets over a 1"-thick aluminum honeycomb core with a nominal density of 3.10 lb/ft^3. The facesheets were fabricated using 8 plies of carbon-fiber tape and were attached to the aluminum core using epoxy film adhesive. The nominal mass per unit area of the panels is 1.35 lb/ft^2. The measured dimensions and mass of the panels are slightly different than the nominal values, and are therefore included in Table 5 in Appendix B.

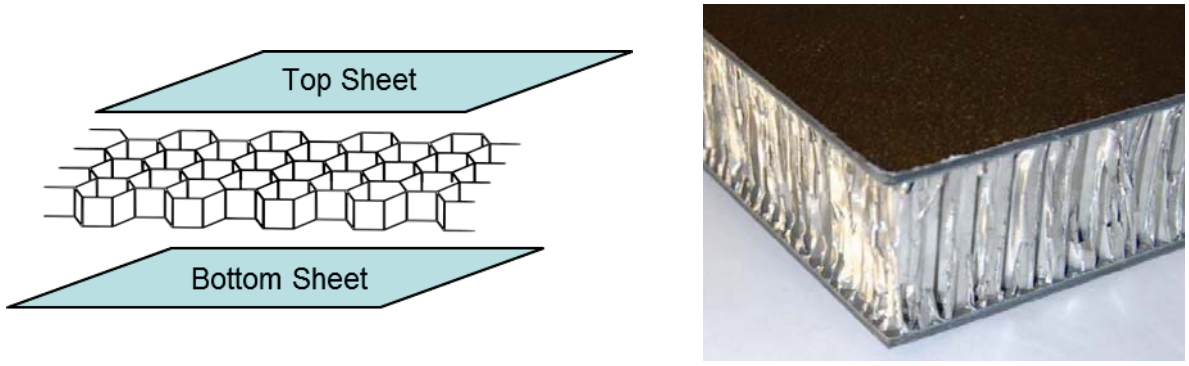

Figure 7: Expanded view (left) and photograph (right) of the honeycomb panel.

Melamine Foam

A large number of tests have been performed over the past several years to identify the baseline acoustic treatment for the SLS payload fairing [5,6,7]. This has resulted in a very large database for various treatment combinations including, but not limited to, melamine foam with different coversheets. For the tests documented in this report, 4”-thick melamine foam (Soundfoam ML ULb manufactured by Soundcoat) was tested with, in some cases, a porous, non-woven fabric coversheet called SoundTex. Nominal properties for the foam and coversheet are included in Table 7 in Appendix C. While most of the tests were performed with foam slabs that covered the entire top surface of the panel(s), 2 transmission loss tests and 2 absorption tests were performed using 4”-thick foam strips that were 8” wide and 48” long. These strips, shown in Figure 8, did not have a coversheet and were placed on the TCC panel(s) between the rows of inlets. When installed in this way, the foam strips covered 50% of the top surface of the panel(s).

Figure 8: Melamine foam slabs with and without a SoundTex coversheet (left) and melamine foam strips (right).

Test Setup and Measurements

The performance of noise treatment is often quantified in terms of noise reduction, which is the difference between the exterior and interior sound pressure levels. When simplifying

assumptions are made regarding the characteristics of the sound field and the interior absorption, then noise reduction can be approximated as

$$NR \approx TL + 10\log_{10}(\bar{\alpha}) \quad (1)$$

where TL is the sound transmission loss, and $\bar{\alpha}$ is the average sound absorption coefficient in the vehicle interior. While noise reduction is difficult to measure without a mock-up of the vehicle compartment, sound transmission loss and sound absorption can both be measured in the laboratory. Therefore, to evaluate the acoustic performance of the TCC structure, both sound transmission loss tests and sound absorption tests were performed at the Riverbank Acoustical Laboratories (RAL), located in Geneva, Illinois on October 19-22, 2015. Absorption tests were performed in accordance with the American Society for Testing and Materials (ASTM) C423 standard, "Standard Test Method for Sound Absorption and Sound Absorption Coefficients by the Reverberant Room Method" [8]. Similarly, transmission loss tests were performed according to the ASTM E90 standard, "Standard Test Method for Laboratory Measurement of Airborne Sound Transmission Loss of Building Partitions and Elements" [9].

Absorption Tests

Absorption tests were performed in a relatively large 10,311 ft^3 reverberant room (Room 0). The room had a sound source in the corner as well as static and rotating diffusers. During testing, pressure signals were acquired with a single 0.5"-diameter diffuse field microphone on a centrally located rotating boom. The absorption tests were conducted in Room 0 in conformance with the requirements of ASTM C423-09a, whereby the room decay rate was determined by averaging the band limited reverberation decay rates resulting from a series of microphone-measured noise burst and decay events [8]. The absorption area was then calculated using the Sabine formula, in accordance with ASTM C423, and the absorption coefficient was found by dividing the absorption area by the top-facing surface area of the treatment.

Fourteen absorption tests were performed in this phase of the testing. Table 1 lists each configuration along with three additional configurations (in italics), which were completed in an earlier set of tests by McNelis and Hughes [7]. The additional tests are included in this report for comparison purposes.

Table 1: Absorption test matrix.

Index	Report #	Panel	Tuning	Inlets	Foam	Foam Mounting	Size
1	A15-294	TCC	200-315 Hz	Closed	None	n/a	8’ x 8’
2	A15-295	TCC	200-315 Hz	Open	None	n/a	8’ x 8’
3	A15-296	TCC	200 Hz	Closed	None	n/a	8’ x 8’
4	A15-297	TCC	200 Hz	Open	None	n/a	8’ x 8’
5	A15-298	TCC (repositioned)	200 Hz	Closed	None	n/a	8’ x 8’
6	A15-299	TCC (repositioned)	200 Hz	Open	None	n/a	8’ x 8’
7	A15-300	TCC	200 Hz	Closed	4" ML ULb with SoundTex Coversheet	2” Spacer	8’ x 8’
8	A15-301	TCC	200 Hz	Open	4" ML ULb with SoundTex Coversheet	2” Spacer	8’ x 8’
9	A15-302	TCC	200 Hz	Open	4” ML ULb	2” Spacer	8’ x 8’
10	A15-303	TCC	200 Hz	Closed	4” ML ULb	2” Spacer	8’ x 8’
11	A15-304	TCC	200 Hz	Closed	4” ML ULb Strips	On Panel	8’ x 8’
12	A15-305	TCC	200 Hz	Open	4” ML ULb Strips	On Panel	8’ x 8’
13	A15-306	TCC	200 Hz	Closed	4” ML ULb	On Floor	(2x) 8’ x 8’
14	A15-307	TCC	200 Hz	Open	4” ML ULb	On Floor	(2x) 8’ x 8’
15	*A15-180*	*Honeycomb*	*n/a*	*n/a*	*None*	*n/a*	*8’ x 8’*
16	*A15-186*	*None*	*n/a*	*n/a*	*4” ML ULb with SoundTex Coversheet*	*On Floor*	*8’ x 8’*
17	*A15-187*	*None*	*n/a*	*n/a*	*4” ML ULb with SoundTex Coversheet*	*2” Spacer*	*8’ x 8’*

For the absorption tests, all three panels were placed next to each other on the floor of the test chamber, as shown in Figure 9. This produced a square, 8’ by 8’, test article that met the C423-09a size and shape requirements. The seam between individual panels was sealed with masking tape, and the outer perimeter of the panels was sealed with wood and metal framing. All of the absorption tests that included the TCC panels were performed in pairs. In one test, the inlets were sealed with masking tape, while a second test was performed with open inlets, as shown by the two photos in Figure 9. Performing the tests in pairs made it easier to isolate the effect of the resonator array on a given treatment configuration.

Figure 9: TCC panels with closed inlets corresponding to tests A15-294 and A15-296 (left) and open inlets corresponding to A15-295 and A15-297 (right).

The first 6 tests in the test matrix were performed with only the TCC panels. The purpose of these tests was to quantify the change in absorption attributed to the resonator array. The first two tests were performed with 35% of the resonators tuned for 200 Hz, 35% tuned for 250 Hz, and 30% tuned for 315 Hz. Following those tests, the panels were retuned and all subsequent tests were performed with 100% of the resonators tuned for 200 Hz.

Tests 7-10 included melamine foam, with a coversheet in some cases, on 2" spacers above the TCC panels. The expanded polyethylene foam plugs that were used to seal the chambers in the TCC panel were also used as the 2" spacers, as shown in Figure 10. The spacers were adhered to the panel using double sided tape and then the foam was placed on top of the spacers. The edges of the assembly were sealed with wood and metal framing, as shown in Figure 11. The figure shows the configuration with the ultra-light melamine foam (on the left), and the configuration with the SoundTex coversheet on top of the foam (on the right).

Figure 10: TCC panel with 2" spacers used in tests A15-302, A15-303, A15-304, and A15-305 (left) and 4" of foam on the spacers (right).


Figure 11: Foam over TCC panels depicting the test setup for A15-302 and A15-303 (left), and coversheet over foam showing the test setup for A15-300 and A15-301 (right).

Tests 11 and 12 were performed using foam strips. The foam was placed on the panel as shown in the photo on the left in Figure 12. Tests 13 and 14 were performed with the foam slab and the TCC panels at separate locations on the floor of the reverberant chamber, as shown in the photo on the right in Figure 12. This configuration was chosen to investigate possible interactions between resonator performance and foam proximity.


Figure 12: Foam strips on TCC panels showing the test setup for A15-304 (left), and foam and panels separated corresponding to A15-306 (right).

The final three tests listed in Table 1 are described in detail by McNelis and Hughes [7]. Test 15 was performed with a bare honeycomb panel on the floor of the reverberant chamber. In contrast, Tests 16 and 17 were performed without any panel. In those tests, the foam (with a coversheet) was placed directly on the floor, or on 2” spacers above the floor. The perimeter of the foam was sealed using wood and metal framing in both cases.

Transmission Loss Tests

Transmission loss (TL) tests were performed using two adjacent reverberant chambers as described in ASTM E90-09. The chambers used for this round of tests were 6,297.6 ft^3 (Room 2) and 4,929.5 ft^3 (Room 3). The two chambers were coupled through a 4’ by 8’ (or smaller) opening. The size of the opening could be reduced using a filler wall constructed of concrete and sealed with dense mastic or clay. Both rooms included a sound source in the corner as well as static and rotating diffusers. During testing, pressure signals were acquired with a single 0.5”-diameter diffuse field microphone on a centrally located rotating boom. The test article was placed in the opening between the two rooms. The source room was ensonified with steady-state broadband noise to approximately 105 dB OASPL. The space and time averaged room levels were then measured with the microphone on the rotating boom and the absorption area of the receiving room was found using the procedure outlined in ASTM C423-09a. The transmission loss of the test article was then found using an expression that accounts for the average sound pressure

level in the source and receiving rooms as well as the absorption area of the receiving room as described in ASTM E90-09.

Sixteen transmission loss tests were performed in this phase of testing. Table 2 lists each configuration along with three additional configurations (in italics), which were completed prior to the start of the tests. Test 17 had been conducted as a standard checkout test by the laboratory. Tests 18 and 19 were completed and documented by McNelis and Hughes in 2015 [7]. All three additional tests are included in this report for comparison purposes. In all of the transmission loss tests except Tests 1 and 17, the smaller of the two reverberant chambers (Room 3) was used as the source room and the larger chamber (Room 2) was used as the receiving room. While it should not matter which room is used as the source and receiving rooms, the tests were performed in this way to better represent the flight configuration with the treatment facing the receiving room.

Table 2: Transmission loss test matrix.

Index	Report #	Panel	Tuning	Inlets	Foam	Foam Mounting	Size
1	TL15-399	0.10" Thick Mass-Loaded Vinyl	n/a	n/a	None	n/a	4’ x 4’
2	TL15-400	TCC	200 Hz	Closed	None	n/a	4’ x 4’
3	TL15-401	TCC	200 Hz	Open	None	n/a	4’ x 4’
4	TL15-402	Honeycomb	n/a	n/a	None	n/a	4’ x 4’
5	TL15-403	TCC	200-315 Hz	Closed	None	n/a	4’ x 8’
6	TL15-404	TCC	200-315 Hz	Open	None	n/a	4’ x 8’
7	TL15-405	TCC	200 Hz	Closed	None	n/a	4’ x 8’
8	TL15-406	TCC	200 Hz	Open	None	n/a	4’ x 8’
9	TL15-407	TCC	200 Hz	Closed	4” ML ULb	2” Spacer	4’ x 8’
10	TL15-408	TCC	200 Hz	Open	4” ML ULb	2” Spacer	4’ x 8’
11	TL15-409	TCC	200 Hz	Closed	4" ML ULb with SoundTex Coversheet	2” Spacer	4’ x 8’
12	TL15-410	TCC	200 Hz	Open	4" ML ULb with SoundTex Coversheet	2” Spacer	4’ x 8’
13	TL15-411	TCC	200 Hz	Open	4” ML ULb	1” Spacer	4’ x 8’
14	TL15-412	TCC	200 Hz	Closed	4” ML ULb	1” Spacer	4’ x 8’
15	TL15-413	TCC	200 Hz	Closed	4” ML ULb Strips	On Panel	4’ x 8’
16	TL15-414	TCC	200 Hz	Open	4” ML ULb Strips	On Panel	4’ x 8’
17	*TL15-102*	*0.10" Thick Mass-Loaded Vinyl*	*n/a*	*n/a*	*None*	*n/a*	*4’ x 8’*
18	*TL15-266*	*Honeycomb*	*n/a*	*n/a*	*None*	*n/a*	*4’ x 8’*
19	*TL15-273*	*Honeycomb*	*n/a*	*n/a*	*4" ML ULb with SoundTex Coversheet*	*On Panel*	*4’ x 8’*

The first four tests were performed using the smaller 4’ by 4’ test articles. Therefore, a filler wall was used to reduce the size of the opening to accommodate these test articles, as shown in Figure 13. These tests had two purposes. First, they could be used to assess the impact of test article size on measured transmission loss, and second, the results could be directly compared with transmission loss tests carried out in a different facility that can only accommodate 4’ by 4’ panels.

Figure 13: Smaller 4' by 4' mass-loaded vinyl sample corresponding to test TL15-399 (left), and smaller 4' by 4' TCC panel with closed inlets showing the setup used in TL15-400 (right).

Tests 5-8 were conducted using the larger 4' by 8' TCC panels. Once again, the tests conducted with the TCC panels were performed in pairs. In one test the inlets were sealed with masking tape, while a second test was performed with open inlets, as shown in Figure 14. This made it easier to isolate the effect of the resonator array on a given treatment configuration.

Figure 14: Larger 4' by 8' TCC panel with closed inlets corresponding to TL15-403 and TL15-405 (left), and open inlets corresponding to TL15-404 and TL15-406 (right).

Tests 9-14 were conducted using either 1'- or 2"-tall closed-cell foam spacers. Once again, the polyethylene foam plugs that were used to seal the chambers in the TCC panel were also used as the spacers. The spacers/plugs were attached to the panel using double sided tape. Since the plugs were nominally 1" thick and 2" tall, the appropriate gap was achieved by either mounting the plugs on their side or upright as shown in Figure 15. The melamine foam was then pushed into position and held in place with dense mastic around the perimeter. The photo on the left in Figure 16 shows the exposed surface of the melamine foam installed in the TL window while the figure on the right shows the SoundTex coversheet.

Figure 15: Foam spacers on the TCC panel. One-inch tall spacers (left) were used in tests TL15-411 and TL15-412, while two-inch tall spacers (right) were used in tests TL15-407, TL15-408, TL15-409, and TL15-410.

Figure 16: Melamine foam over the TCC panel showing the setup used in TL15-407, TL15-408, TL15-411, and TL15-412 (left), and foam with the SoundTex coversheet corresponding to TL15-409 and TL15-410 (right).

Foam strips were also tested as shown in the photo on the left in Figure 17. The foam was placed directly on the panel but was staggered so that it would not cover the inlets. Figure 17 also shows the back side of the panel, facing the source room. The bead of mastic/clay is visible around the perimeter of the panel. The mastic was used to seal both sides of the assembly, eliminating gaps.

Figure 17: Foam strips installed on the TCC panel with open inlets corresponding to TL15-414 (left), and opposite side of TCC panel facing the source room, which is representative of all 4' by 8' TCC tests (right).

Modeling Approach

This section briefly describes the modeling approach. While a detailed description is beyond the scope of this report, a high-level overview will be provided along with references that contain additional details. Specifically, a wave-based analytical modeling approach, referred to as the transfer matrix method (TMM), was used to generate absorption and transmission loss predictions for the configurations tested. Note that these predictions incorporate corrections that account for the finite size of the test articles. This results in absorption coefficients that can exceed unity and an increase in transmission loss particularly at low frequencies [10,11,12].

Transfer Matrix Method

The transfer matrix method is a general modeling approach used to analyze wave propagation through layered media. The approach, as described by Allard and Atalla [10], is a powerful and efficient modeling framework for predicting wave propagation through complex multilayer systems consisting of combinations of fluid, elastic solid, and poroelastic materials, as well as thin plates, membranes, and meshes. For this discussion, however, the focus is restricted to combinations of fluid layers, thin partitions, and 2D arrays of resonators. In addition, the layers are assumed to be homogeneous and transversely isotropic, and initially it is also assumed that the layers are infinitely large in the in-plane dimensions. The system is assumed to be excited by a plane wave incident at angle θ, as depicted in Figure 18, and the pressure and normal component of velocity (i.e., in the z-direction) on either side of the system are represented as p, v_z and p', v_z'. If the system is linear, then the acoustic pressure and particle velocity on either side of the multilayer system are related by

$$\begin{matrix} p \\ v_z \end{matrix} = \begin{bmatrix} T_{11} & T_{12} \\ T_{21} & T_{22} \end{bmatrix} \begin{matrix} p' \\ v_z' \end{matrix} \tag{2}$$

where $T = \begin{bmatrix} T_{11} & T_{12} \\ T_{21} & T_{22} \end{bmatrix}$ is the global transfer matrix. If we further restrict this discussion to layers that are of the same nature, then the global transfer matrix is simply the product of the transfer matrices for the individual layers. For example, the global transfer matrix for the 3-layer system depicted in Figure 18 can be found as

$$T = T_a \cdot T_b \cdot T_c = \begin{bmatrix} T_{11} & T_{12} \\ T_{21} & T_{22} \end{bmatrix} \tag{3}$$

where T_a, T_b, and T_c represent local transfer matrices for each layer. Recall that our focus is on combinations of fluid layers, thin partitions, and 2D arrays of resonators. Therefore, local transfer matrices will be defined for each of these types, starting with the fluid layer.

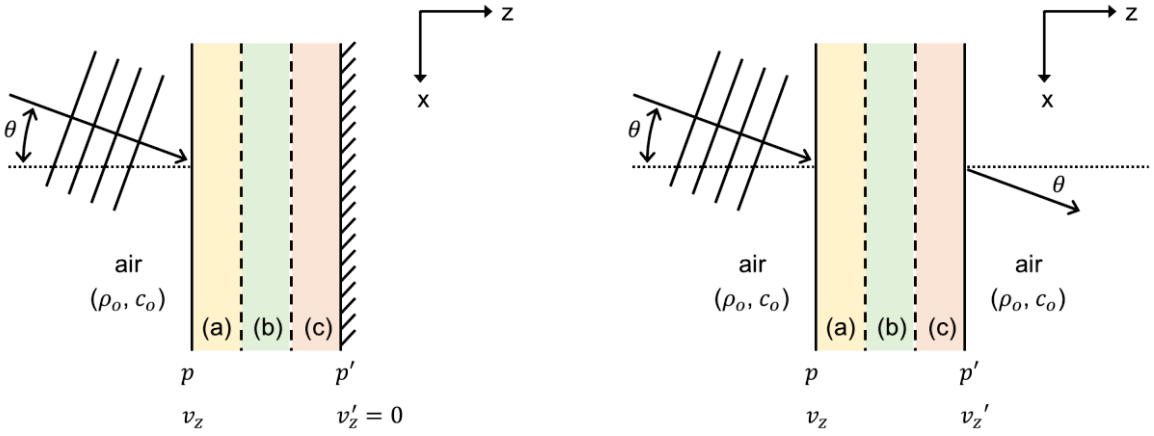

Figure 18: Plane wave propagation through a multilayer system configured for absorption (left) and transmission loss (right).

Fluid Layers

In this study, the air gaps and the foam were both modeled as fluid layers. The local transfer matrix for a fluid layer can be expressed as

$$T_f = \begin{bmatrix} \cos(k_z h) & \mathrm{j}\dfrac{\omega\rho_f}{k_z}\sin(k_z h) \\ \mathrm{j}\dfrac{k_z}{\omega\rho_f}\sin(k_z h) & \cos(k_z h) \end{bmatrix} \tag{4}$$

where $k_z = \left(k_f^2 + k_0^2 \sin^2\theta\right)^{1/2}$ is the z-component of the wavenumber in the fluid layer, k_f is the wavenumber within the layer, k_o is the wavenumber in the incident fluid (air in this case), h is the layer thickness, ω is angular frequency, and ρ_f is the density of the fluid within the layer. Note that $e^{j\omega t}$ time convention has been assumed here and throughout the rest of this report.

Air is modeled as a fluid with real-valued and frequency-independent density and speed of sound. Similarly, foam can be represented as an equivalent fluid by specifying frequency-dependent and complex-valued properties. For the predictions shown in this document, the properties for ML ULb foam were estimated using the empirical Delany-Bazley-Miki model [13] with a flow resistivity of 18 lbf-s/ft^4 (9400 Ns/m^4) based on previous tests [11]. Using this model, the characteristic impedance and propagation constant can be calculated as

$$z_f = \rho_o c_o\left(1 + 0.07X^{-0.632} - j(0.107X^{-0.632})\right) \tag{5}$$

and

$$\Gamma_f = k_o\left(0.16X^{-0.618} + j(1 + 0.109X^{-0.618})\right) \tag{6}$$

where ρ_o is the density of air, c_o is the speed of sound of air, $k_o = \omega/c_o$ is the wavenumber in air, $X = \rho_o f/\sigma$, and σ is the specific flow resistivity in units of Ns/m^4. The wavenumber and density in the foam layer can then be calculated as

$$k_f = -\mathrm{j}\Gamma_f \tag{7}$$

and

$$\rho_f = z_f k_f/\omega \tag{8}$$

Thin Partitions

The structural panels and the coversheet on the foam were all modeled as thin partitions. This implies that the layer is thin relative to the acoustic wavelength and wave propagation within the layer (in the z-direction) is not explicitly represented. Instead, the layer is characterized by its specific impedance. The local transfer matrix for a thin partition can be expressed as

$$T_p = \begin{bmatrix} 1 & z_p \\ 0 & 1 \end{bmatrix} \tag{9}$$

where z_p is the specific impedance of the partition. For example, the specific impedance of a thin elastic plate in flexure can be written as [14]

$$z_p = j\omega m_s \left[1 - \frac{D k_x^4}{\omega^2 m_s}\right] \tag{10}$$

where m_s is the mass per unit area, $D = Eh^3/\left(12(1-\nu^2)\right)$ is the flexural rigidity, E is Young's modulus, h is thickness, ν is Poisson's ratio, and $k_x = k_o \sin\theta$ is the x-component of the wavenumber in the incident fluid. Similar equations were used to model the structural panels and coversheet as described in the following subsections.

TCC (Without Resonators)

Since the TCC panels have a corrugated core, the bending stiffness is highly directional. To capture this behavior, the impedance of the TCC panel was approximated using a more general expression for a thin orthotropic plate in flexure [15]

$$z_p = j\omega m_s \left(1 - \frac{D_x k_x^4}{\omega^2 m_s} - \frac{2D_{xy} k_x^2 k_y^2}{\omega^2 m_s} - \frac{D_y k_y^4}{\omega^2 m_s}\right) \tag{11}$$

where $k_x = k_o \sin(\theta)\cos(\varphi)$, $k_y = k_o \sin(\theta)\sin(\varphi)$, D_x is the bending stiffness in the compliant cross direction, D_y is the bending stiffness in the stiff axial direction, and $D_{xy} = \sqrt{D_x D_y}$. In this case, φ is the azimuthal angle as shown in Figure 19. The bending stiffness was estimated based on a combination of tests and detailed FE models [16]. The resulting stiffness estimates are included in Appendix A. Damping was incorporated in this model by multiplying the bending stiffness estimates by $(1 + j\eta)$, where η is the damping loss factor.

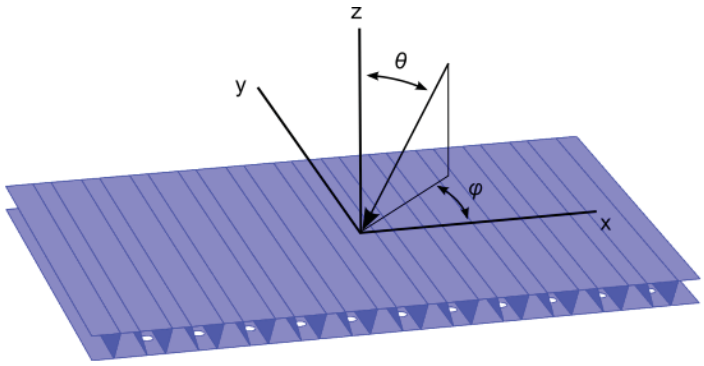

Figure 19: Angle convention assumed for the TCC model.

Mass-Loaded Vinyl

The mass-loaded vinyl was represented as a limp mass, which is characterized by its mass per unit area. In this case, the specific impedance expression given by Eqn. (10) was used with the bending stiffness set to zero.

Coversheet

The coversheet was modeled as a limp porous layer, which can be represented as two impedances in parallel

$$z_{cs} = \frac{1}{1/z_p + 1/z_h} \tag{12}$$

where z_p is the impedance of a limp panel, and z_h is the acoustic impedance of a rigid porous sheet. In this case, z_h was set equal to the flow resistance of the porous layer. The mass per unit area and flow resistance for the coversheet are included in Table 8 in Appendix C.

Sandwich Honeycomb

Finally, the honeycomb sandwich panel was modeled using a formulation proposed by Narayanan and Shanbhag [17]. Specifically, the model captures the forced response (i.e., non-resonant response) of a symmetric sandwich panel with isotropic facesheets over a transversely isotropic core. The derivation assumes that the bending behavior is controlled by the facesheets, the core is stiff such that there is no relative motion between the two facesheets and the core in the transverse direction (i.e., z-direction), and the shear response is controlled by the core. Given these assumptions, the specific impedance of the panel can be written in a form very similar to Eqn. (10), but with an additional term that accounts for the transverse shear stiffness of the core

$$z_p = j\omega m_s \left[1 - \frac{D_t k_x^4}{\omega^2 m_s}\left(1 + \frac{gY}{k_x^2 + g}\right)\right] \tag{13}$$

where $D_t = 2Eh_{fs}^3/\left(12(1-\nu^2)\right)$ accounts for the flexural rigidity of both facesheets, E is Young's modulus of the facesheet, h_{fs} is the thickness of one facesheet, ν is Poisson's ratio of the facesheet, $k_x = k_o \sin\theta$ is the x-component of the wavenumber in the incident fluid, $Y = 3\left(1 + h_c/h_f\right)^2$ is a geometric parameter, $g = 2G(1-\nu^2)/\left(Eh_f h_c\right)$ is a shear parameter, G is the shear modulus of the core, and h_c is the thickness of the core. Damping was included in this model by multiplying both Young's modulus and the shear modulus by $(1 + j\eta)$, where η is the damping loss factor. The dimensions and mechanical properties for the honeycomb panels are included in Appendix B.

Resonator Array

The acoustic resonators embedded within the TCC panel are modeled as a separate layer. Specifically, the local transfer matrix for an array of resonators is expressed as

$$T_{ra} = \begin{bmatrix} 1 & 0 \\ 1/z_{ra} & 1 \end{bmatrix} \tag{14}$$

where z_{ra} is the effective impedance of the resonator array.

To calculate the effective impedance of the array, it was first necessary to estimate the impedance of individual resonators. The resonators embedded within the corrugated-core panel consist of long trapezoidal cavities with an inlet near one end. The fact that the inlet is in the side of the cavity, and not at the end, makes little difference at low frequencies [18]. Therefore, the input impedance of the resonators can be estimated by combining the impedance of the long cavity with the impedance of the inlet, and can be expressed as [3]

$$z_{ri} = z_i + z_c = j\omega\rho_o L_n - j\frac{\rho_o c_o}{S_c}\cot(k_o L_c) S_i + R \tag{15}$$

where S_c is the cross-sectional area of the cavity, L_c is the length of the cavity, S_i is the cross-sectional area of the inlet, and L_n is the effective length of the neck. The effective length of the neck equals the thickness of the facesheet plus an additional $(8r/(3\pi))$ interior end correction term to account for the internal fluid loading, where r is the radius of the circular inlet [19]. The term, R, is a resistance term that accounts for the thermal and viscous losses in the cavity and inlet. This term affects the quality factor or lossiness of the resonator and was set to 2.0 lb/(ft^{2}s) based on previous studies [20].

The input impedance of the resonator is important, however, it is also necessary to account for the radiation impedance of the acoustic wave propagated away from the resonator. Since the inlet is circular, the radiation impedance for a baffled circular piston can be used to approximate the radiation impedance. At low frequencies, where $kr \ll 1$, the specific acoustic radiation impedance can be approximated as [19]

$$z_{rad} = jk\rho c\, 8r/(3\pi) + \rho c(kr)^2/2 \tag{16}$$

The imaginary part of Eqn. (16) essentially represents a mass loading on the resonator, which decreases the resonance frequency. The real part of Eqn. (16) is an additional loss term accounting for the power radiated into the fluid surrounding the resonator. The total impedance of the resonator coupled to the surrounding fluid can then be written as

$$z_r = z_{ri} + z_{rad} \tag{17}$$

Note that this expression was derived for an isolated resonator. If an array of resonators is considered, and the separation distance between the inlets is less than half a wavelength, then the mutual interaction between neighboring resonators will increase the radiation impedance [21]. This will reduce the natural frequency of the resonators and add damping to the system. However, since the interaction between resonators is expected to be a second order effect, it is not explicitly included in the models presented in this report. Once the total impedance for an isolated resonator is known, then the effective impedance for the resonator array can calculated as

$$z_{ra} = z_r/(S_i N/ab) \tag{18}$$

where N is the total number of resonators in the array, a is the width, and b is the length of the array. Note that the denominator of Eqn. (18) defines the ratio of the total area of all resonator inlets relative to the total surface area of the array.

Acoustic Metrics

As previously discussed, when all of the layers of noise treatment are of the same nature, the global transfer matrix can simply be calculated as the product of the local transfer matrices. The acoustic indicators, specifically absorption and transmission loss, can then be calculated in terms of the coefficients of the global transfer matrix.

Absorption

The absorption coefficient is derived assuming the multilayer treatment is terminated by a rigid wall, as depicted on the left in Figure 18. In this case, the plane wave reflection coefficient can be expressed in terms of the coefficients of the global transfer matrix as

$$R = \frac{T_{11}/T_{21} - \rho_o c_o/\cos\theta}{T_{11}/T_{21} + \rho_o c_o/\cos\theta} \tag{19}$$

where T_{11}/T_{21} is the surface impedance of the sample, often expressed as z_s. The angle dependent absorption coefficient can then be calculated as

$$\alpha(\theta) = 1 - |R|^2 \tag{20}$$

However, since the transfer matrix approach assumes that the layers are infinite in the lateral directions, the resulting prediction tends to be biased relative to measurements collected with finite size test articles. To account for the finite size of the test article, the influence of the radiation impedance of the finite test article is included in the calculation. Specifically, the diffuse field absorption coefficient is calculated as [10,11]

$$\alpha = \frac{\int_0^{2\pi}\int_0^{\pi/2} W_{abs}\sin\theta\, d\theta d\varphi}{\int_0^{2\pi}\int_0^{\pi/2} W_{inc}\sin\theta\, d\theta d\varphi} \tag{21}$$

where the incident power is defined as

$$W_{inc} = \frac{|\hat{p}_{inc}|^2 ab}{2z_o}\left(\frac{4\cos\theta}{\left|1 + \frac{z_{rad}}{z_o}\cos\theta\right|^2}\right) \tag{22}$$

and the absorbed power is expressed as

$$W_{abs} = \frac{|\hat{p}_{inc}|^2 ab}{2z_o}\left(\frac{4\mathrm{Re}\left(\frac{z_s}{z_o}\right)}{\left|\frac{z_s}{z_0}+\frac{z_{rad}}{z_o}\right|^2}\right) \tag{23}$$

In this case, $|\hat{p}_{inc}|$ is the amplitude of the incident plane wave, a is the width of the test article, b is the length of the test article, $z_o = \rho_o c_o$ is the characteristic impedance of air, z_s is the surface impedance of the sample, and z_{rad}/z_o is the normalized radiation impedance seen by the finite absorber. The normalized radiation impedance can be calculated as [22]

$$\frac{z_{rad}}{z_o} = \frac{jk_o}{2\pi ab}\int_0^a\int_0^b 4\cos(k_o\mu_x\kappa)\cos\left(k_o\mu_y\tau\right)\frac{e^{-jk_o\sqrt{\kappa^2+\tau^2}}}{\sqrt{\kappa^2+\tau^2}}(a-\kappa)(b-\tau)d\tau d\kappa \tag{24}$$

where $\mu_x = \sin(\theta)\cos(\varphi)$, $\mu_y = \sin(\theta)\sin(\varphi)$, and κ and τ are dummy variables used in the integration.

Transmission Loss

For the transmission loss derivation, it is assumed that the same fluid, in this case air, is on either side of the system, as depicted on the right in Figure 18. In addition, it is assumed that the fluid is semi-infinite such that plane waves propagate away from the sample without reflections. We can then write an expression for the plane wave sound-power transmission coefficient in terms of the coefficients of the global transfer matrix [23]

$$\tau(\theta) = \frac{4}{|T_{11} + T_{12}\cos\theta/(\rho c) + T_{21}\rho c/\cos\theta + T_{22}|^2} \tag{25}$$

which results in the angle dependent plane wave transmission loss

$$TL(\theta) = 10\log_{10}\left(1/\tau(\theta)\right) \tag{26}$$

Once again, the previous expression was derived for an infinitely large sample, which can result in a bias relative to finite panel measurements. To account for the finite size of the panel in the prediction, the angle dependent transmission coefficient (Eqn. (25)), is updated to account for the finite panel radiation efficiency as [10]

$$\tau_f(\theta,\varphi) = \tau(\theta)\mathrm{Re}\left(\frac{z_{rad}}{z_o}\right)\cos\theta \tag{27}$$

where z_{rad}/z_o is defined in Eqn. (24). The diffuse field transmission coefficient for the finite size panel can then be calculated by integrating the updated plane wave transmission coefficient $\tau_f(\theta,\varphi)$ over all angles of incidence

$$\tau_d = \frac{\int_0^{2\pi}\int_0^{\pi/2}\tau_f(\theta,\varphi)\sin(\theta)\cos(\theta)d\theta\, d\varphi}{\int_0^{2\pi}\int_0^{\pi/2}\sin(\theta)\cos(\theta)d\theta\, d\varphi} \tag{28}$$

Finally, the diffuse field transmission loss can be calculated as

$$TL_d = 10\log_{10}(1/\tau_d) \tag{29}$$

Results and Discussion

This section presents both measurements and predictions. Trends are identified and explanations are provided when possible.

Absorption Results

Diffuse-field (Sabine) absorption coefficient plots are presented in this section for the untreated panels, TCC panels with embedded resonators, acoustic foam, and combined configurations consisting of foam over the TCC panels. Note that while the Sabine absorption coefficient approximates the amount of energy dissipated relative to the energy incident on the test article, this parameter is not always less than one. This is commonly attributed to edge effects

associated with the finite size of the test article, as discussed in numerous references [11,24]. Recall that the size effect is included in the predictions presented in this report.

Untreated Structures

Figure 20 shows the Sabine absorption coefficient for untreated honeycomb and TCC panels. In this case, all of the resonator inlets were sealed with tape, so the measured absorption is attributed to only the structure. As expected, the absorption coefficient for the untreated structures is relatively low, which implies that most of the sound incident on the test articles is reflected and not absorbed. Interestingly however, the 2”-thick TCC panels exhibit increased absorption around 500 Hz. In this frequency range, the structure could be modeled as a type of membrane absorber. However, the absorption is still relatively low and arguably insignificant when compared to the absorption provided by conventional noise control treatments at these frequencies. Consequently, no attempt was made to model the baseline absorption of the structure.

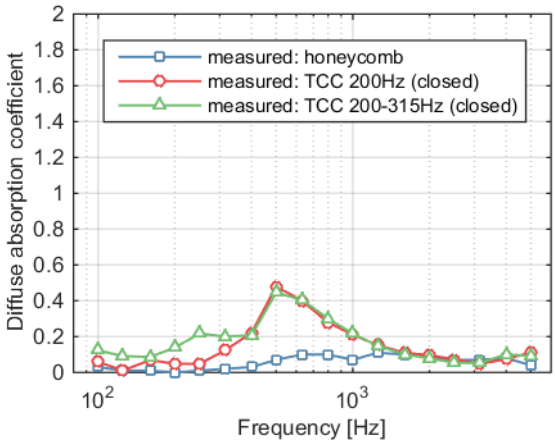

Figure 20: Diffuse (Sabine) absorption coefficient for untreated panels on a hard floor: measurements from tests A15-180, A15-296, and A15-294.

TCC Panels with Resonators

Figure 21 shows the measured (left) and predicted (right) absorption coefficient for the TCC panels with open inlets. Notice that when all of the resonators were tuned for 200 Hz, the Sabine absorption coefficient was slightly larger than one. In contrast, when the natural frequency of the resonators was spread over multiple one-third octave bands, the benefit was spread accordingly. The predictions capture both trends, closely matching the measurements below 400 Hz. However, as mentioned previously, the predictions do not capture the increase due to the structure near 500 Hz evident in the measured data.

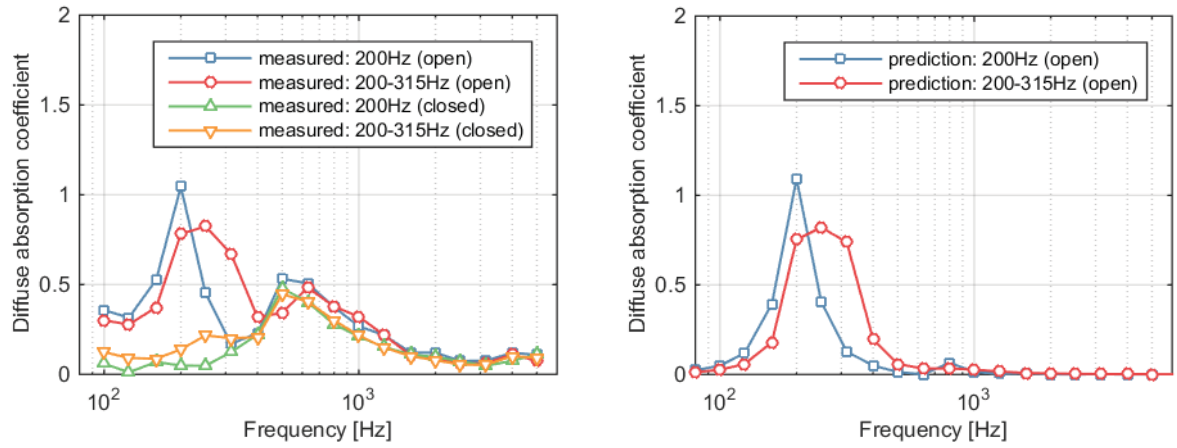

Figure 21: Diffuse (Sabine) absorption coefficient for TCC panels with open inlets: measurements from tests A15-297, A15-295, A15-296, and A15-294 (left figure), and predictions (right figure).

Foam

Several results from earlier foam tests by McNelis and Hughes [7] are included here for comparison purposes. Specifically, Figure 22 shows the absorption coefficient for a 4”-thick foam slab and coversheet with and without an air gap below the foam. Once again, measurements are shown on the left, while predictions are shown on the right. As expected, the Sabine absorption coefficient exceeds unity at some frequencies due to the highly absorptive nature and finite size of the test articles. This trend is also captured, to a lesser degree, by the predictions. The effect of the 2” air gap between the foam and floor is also clearly visible in both the measurements and predictions. Specifically, the air gap shifts the absorption curve to the left at low frequencies.

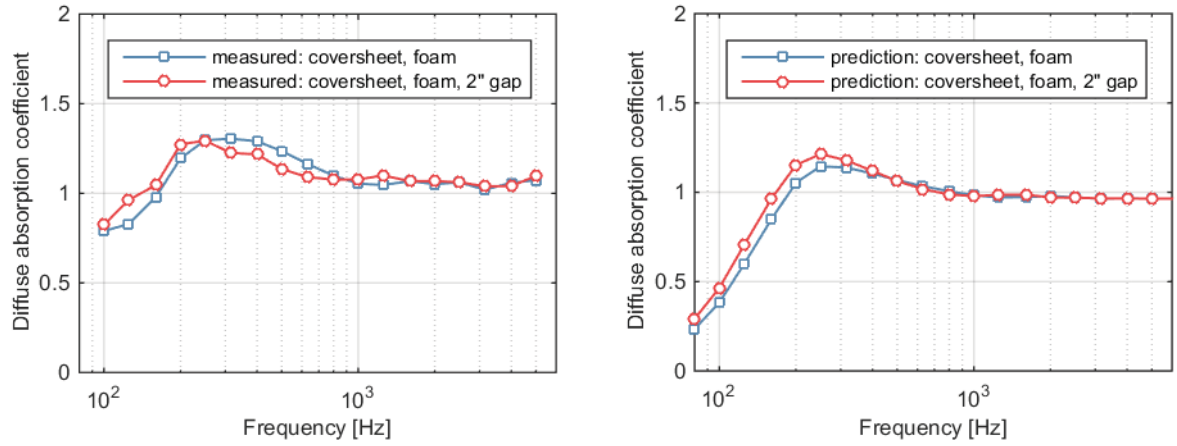

Figure 22: Effect of a 2” spacer on the diffuse (Sabine) absorption coefficient: measurements from tests A15-186 and A15-187 (left figure), and predictions (right figure).

The impact of the coversheet is demonstrated in Figure 23. While the measurements show a clear shift to the left due to the added coversheet, the change is once again apparent, but less pronounced in the predictions. It should be noted that the trend observed in Figure 23 is applicable to the SoundTex coversheet, which is a porous fabric. Non-porous coversheets can have a similar effect at low-frequencies, but tend to reduce the high frequency performance [7].

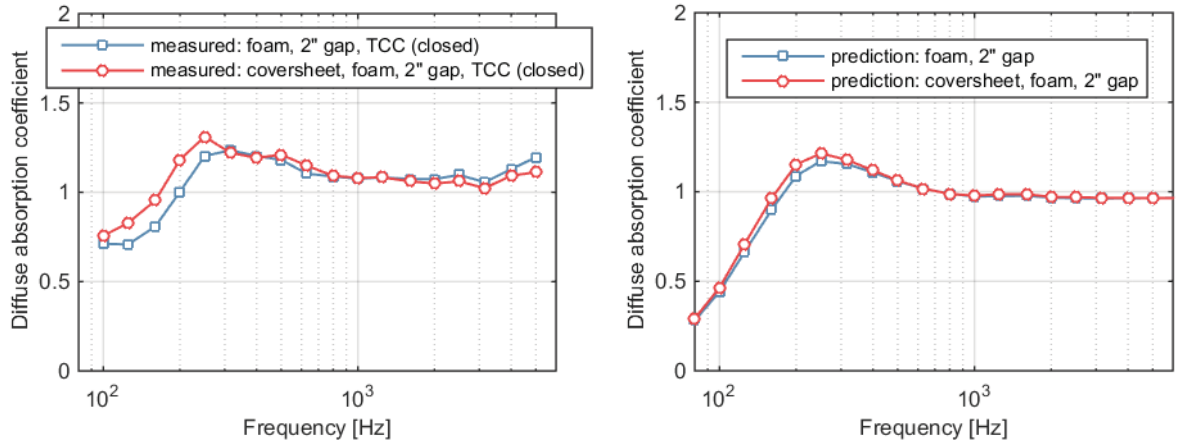

Figure 23: Effect of porous coversheet on the diffuse (Sabine) absorption coefficient: measurements from tests A15-300 and A15-303 (left figure), and predictions (right figure).

Combined Configurations

The combined performance of the foam over the TCC panels is shown in Figure 24. In this case, all of the resonators were tuned for 200 Hz. The figure shows that the combined performance of the foam and resonators is significantly better than either treatment alone below 200 Hz. Above 300 Hz, the performance of the combined treatment is similar to the performance of the foam. However, near 250 Hz the interaction between the foam and resonators resulted in a reduction in absorption relative to the foam treatment. A similar effect is also captured by the model, which allows us to explore other configurations that were not tested. For instance, the orange curve shows the predicted absorption coefficient for foam over TCC panels with the resonators tuned for 200-315 Hz. In this case, the predicted performance of the combined configuration is equal or better than either treatment alone in all one-third octave bands.

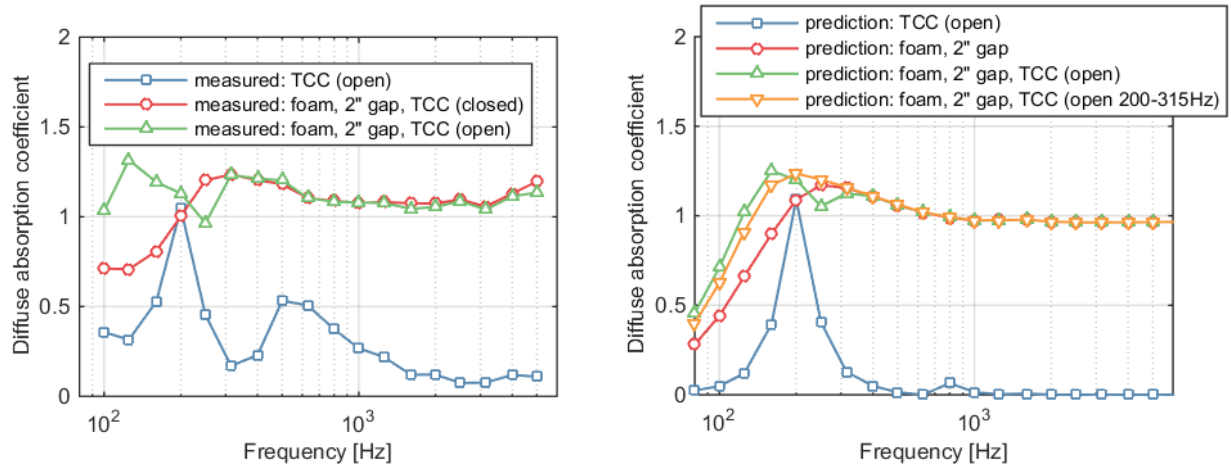

Figure 24: Diffuse (Sabine) absorption coefficient with foam over the TCC panels: measurements from tests A15-297, A15-303, and A15-302 (left figure), and predictions (right figure).

Figure 25 shows the combined performance of the foam, with a coversheet this time, over the TCC panels. The trends are similar to the case previously discussed. However, the low frequency performance is now slightly better due to the addition of the coversheet. Once again, the model captures the relevant trends, and therefore, could be used to optimize the combined configuration based on the noise reduction requirements.

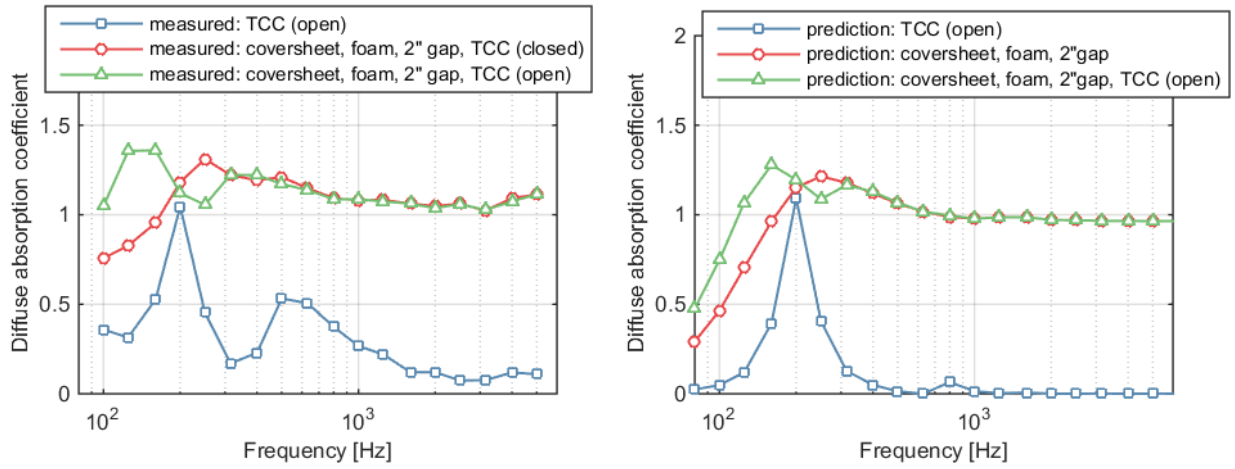

Figure 25: Diffuse (Sabine) absorption coefficient with foam and a coversheet covering the TCC panels: measurements from tests A15-297, A15-300, and A15-301 (left figure), and predictions (right figure).

The absorption coefficient for the configuration with foam strips is shown in Figure 26. Since the foam strips did not cover the inlets, there is less interaction between the resonators and foam. In this case, the combined performance is largely additive. It is valuable to note that at low frequencies the absorption coefficient for the foam strips (red curve in Figure 26) is significantly less than the absorption coefficient for the full foam slab (red curve in Figure 24). While the predictions capture the trends observed in the measurements, the performance of the foam strips is under-predicted relative to measurements. The discrepancy is likely due to the fact that the surface area of the unsealed edges of the foam strips is not included in the model.

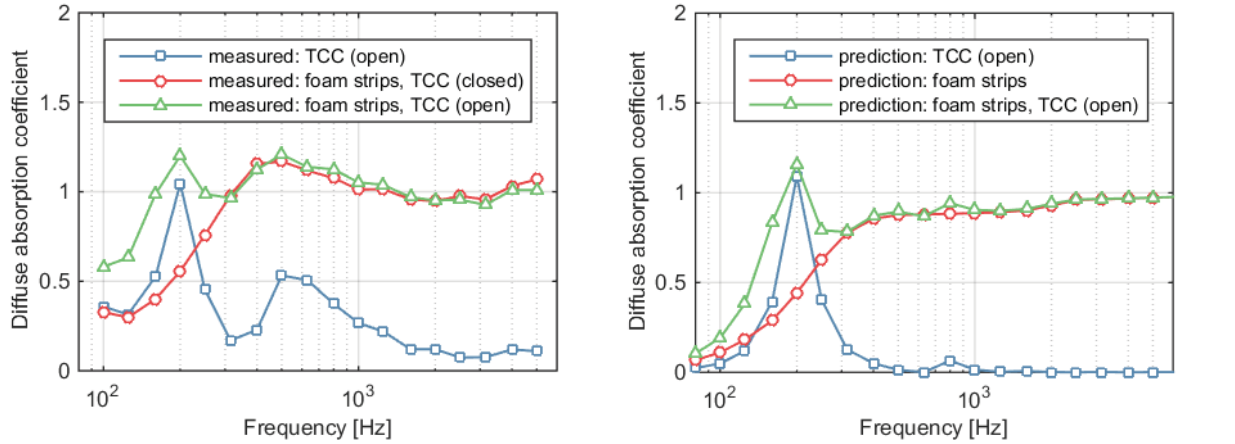

Figure 26: Diffuse (Sabine) absorption coefficient with foam strips over the TCC panels: measurements from tests A15-297, A15-304, and A15-305 (left figure), and predictions (right figure).

An additional test was performed with the foam and TCC panels separated from each other. The purpose of this test was to demonstrate that including foam in the reverberant chamber (away from the TCC panels) would not produce the same combined effect as having the foam on top of the panels. Since the footprint of the combined treatment was twice as large as previous tests, it is useful to consider the measured absorption area of the treatment, rather than the absorption coefficient. Absorption area is defined as the acoustic power absorbed by the treatment divided by the incident intensity (power per unit area). Therefore, absorption area has units of area, and is expressed in this report in ft^2, or Sabins. The absorption area for several configurations is shown in Figure 27. Notice that when the foam and TCC panels are separated, the total absorption area equals the sum of the absorption area of each (as shown on the left in Figure 27). In this case,

there is no frequency shift or complex interaction between the treatments, as seen when the foam is on top of the TCC panels (as shown by the green curve on the right in Figure 27).

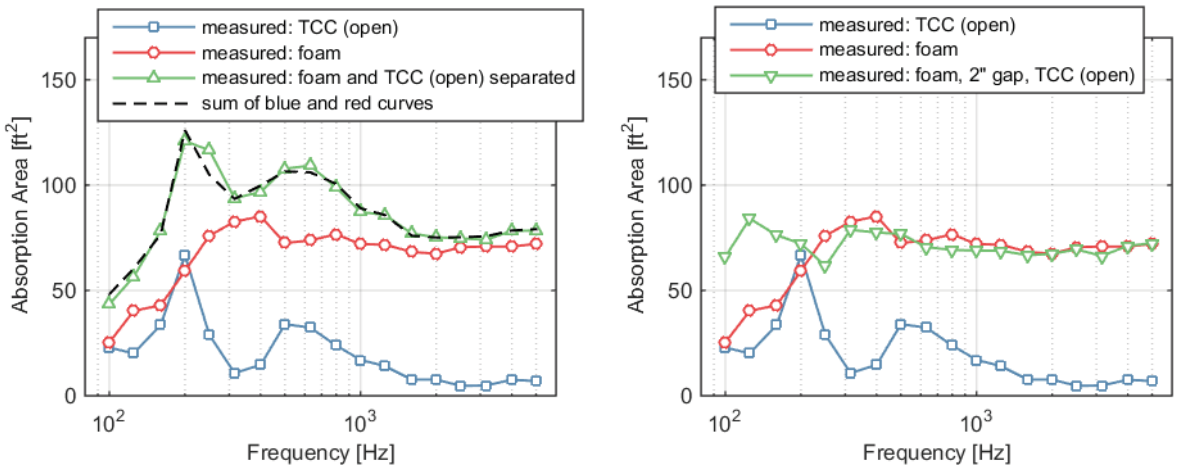

Figure 27: Diffuse absorption area with foam and TCC panels separated: measurements from tests A15-297, A15-306 – A15-296, A15-307, and A15-297 + (A15-306 – A15-296) (left figure), and measurements from tests A15-297, A15-306 – A15-296, and A15-302 (right figure).

Transmission Loss Results

Diffuse-field transmission loss plots are presented next. Results are shown for the untreated structures first, followed by the TCC panels with the resonators active (i.e., open inlets). The effect of the foam is then presented along with the combined configurations with foam over the TCC panels.

Untreated Structures

Figure 28 shows the transmission loss for mass-loaded vinyl. Recall that mass-loaded vinyl is often used for quality control and model validation purposes since the results are typically repeatable and well understood. Therefore, measurements and predictions can be compared to provide a quick check on the appropriate operating range of a facility. In this case, the predictions and measurements match very well at most frequencies. However, the curves diverge below 200 Hz. This implies that one (or more) of the modeling assumptions are not valid in this frequency range. For instance, the divergence could indicate that the room diffusivity becomes inadequate and strong room modes become dominant at these frequencies. However, regardless of the reason, the divergence at low frequencies should be kept in mind when comparing measurements and predictions for other configurations.

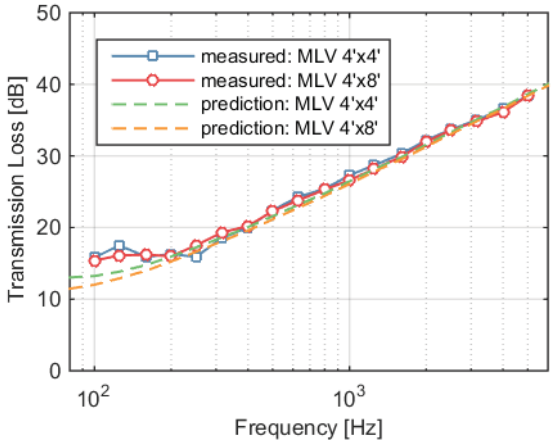

Figure 28: Transmission loss of mass-loaded vinyl from tests TL15-399 and TL15-102 (solid lines), and predictions (dashed lines).

The plot on the left in Figure 29 shows the measured transmission loss for two honeycomb panels: a 4' by 4' panel and a 4' by 8' panel. Below 300 Hz the transmission loss appears to be controlled by the resonant (or modal) behavior of the panels with dips in transmission loss corresponding to structural resonances. Since the size and boundary conditions of the panels affect the location of individual modes, it is not surprising that there is significant low frequency variation. However there are also noticeable differences above 400 Hz. The TL of the smaller panel is approximately 2 dB higher than the TL of the larger panel. This is due, in part, to a manufacturing variability resulting in a difference in mass per unit area. The 4' by 4' panel has a 5% larger mass per unit area than the 4' by 8' panel (1.39 lb/ft^2 versus 1.32 lb/ft^2). However, this difference would be expected to change the TL by less than 0.5 dB. Above the critical frequency, which is approximately 300 Hz for these panels, an increase in structural damping can provide a nearly constant increase in the diffuse-field TL. To demonstrate this, the predictions included in the plot on the right in Figure 29 were generated using damping loss factors of 4% and 8%. Notice that the difference in the predictions is similar to the shift observed in the measurements. The relatively high damping could be attributed, in part to the mastic used to seal around the perimeter of the panels during the test. This material extended from the wall, onto the panel, covering the outer 1" of the panels on both the source and receiving room sides. Since the mastic covered a larger fraction of the 4' by 4' panel, it is possible that the mastic had a larger impact on damping in this case.

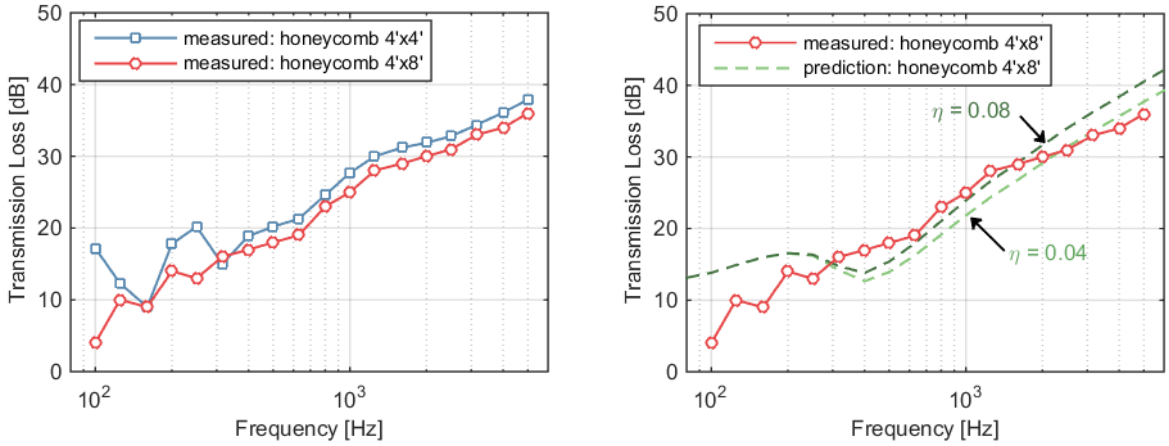

Figure 29: Transmission loss of the honeycomb panels from tests TL15-402 and TL15-266 (solid lines), and predictions (dashed lines).

The plot on the left in Figure 30 shows the measured TL for the 4' by 4' and 4' by 8' TCC panels with inlets closed (i.e., covered with masking tape). Once again, there are noticeable differences in the TL of the two panels. The differences could be attributed, in part, to differences in damping as previously discussed with regard to the honeycomb panels. There are similarities as well though. Both curves have dips or inflection points around 160 Hz, 1-2 kHz, and around 5 kHz. These aspects were found to be caused by multiple coincidences between the acoustic wavelength and panel flexural wavelengths in the axial- and cross-corrugation directions (refer to [16] for more details). For the purposes of this study, however, a thin orthotropic shell formulation with constant flexural rigidities in the axial- and cross-corrugation directions was used that approximates the behavior of the TCC panel at low frequencies. The wavelength coincidence effects at higher frequencies are not captured with this model. Estimates for the flexural rigidities are included in Appendix A. Finally, note that a damping loss factor of 4% was assumed for subsequent TCC panel predictions based on the favorable comparison with measurements, as shown on the right in Figure 30.

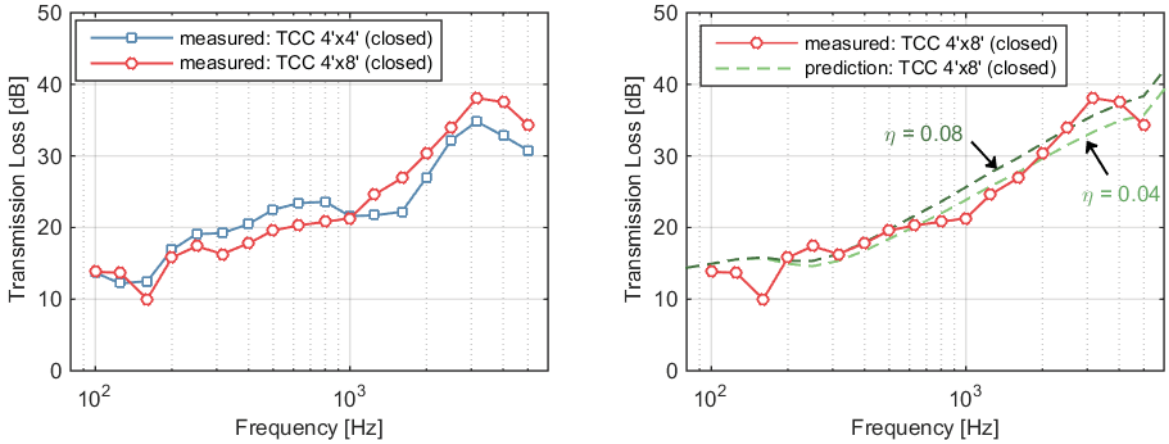

Figure 30: Transmission loss of the TCC panels (with closed inlets) from tests TL15-400 and TL15-405 (solid lines), and predictions (dashed lines).

Figure 31 compares the measured TL for the three different 4' by 8' panels tested. Note that the mass per unit area of the mass-loaded vinyl, honeycomb, and TCC panels are: 1 lb/ft^2, 1.32 lb/ft^2, and 1.54 lb/ft^2, respectively. In other words, the TCC panel is 54% heavier than the MLV and 17% heavier than the honeycomb panel. While the overall trends are similar, the TL of the honeycomb and TCC panels is almost always lower than the TL of the mass-loaded vinyl

despite the fact that the honeycomb and TCC panels are heavier. This trend emphasizes the importance that resonance and coincidence have on TL. Finally note that the low frequency differences in the TL measurements for the honeycomb and TCC panels are not necessarily indicative of the differences one would expect to see on larger structures. This is because the low frequency TL is sensitive to the modal behavior of structure, which depends on the size and boundary conditions of the test article.

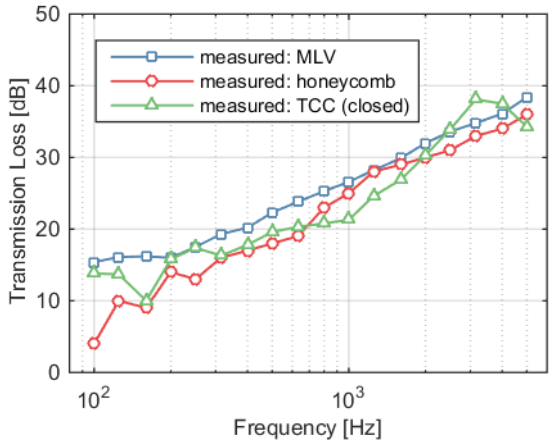

Figure 31: Transmission loss of 4' by 8' panels from tests TL15-102, TL15-266, TL15-405, TL15-406.

TCC Panel with Resonators

Recall that the tests performed with the TCC panels were done in pairs, with both open and closed inlets. This enabled the calculation of Insertion Loss (IL), or the change in TL attributed to the resonators, for each configuration. For example, Figure 32 shows the TL for the 4' by 8' TCC panel with and without the acoustic resonators on the left and the IL for the same panel on the right. In this set of tests, the resonators were all tuned for 200 Hz, which explains why the maximum IL occurs in that one-third octave band. Notice that while the resonators improve the low-frequency TL, there is a penalty at higher frequencies. This is due to the fact that the inlets introduce an additional transmission path through the panel, which becomes significant at high frequencies. However, since the low-frequency acoustic environment often drives the need for noise treatment, it can be desirable to improve low-frequency performance even if there is a penalty at high-frequencies.

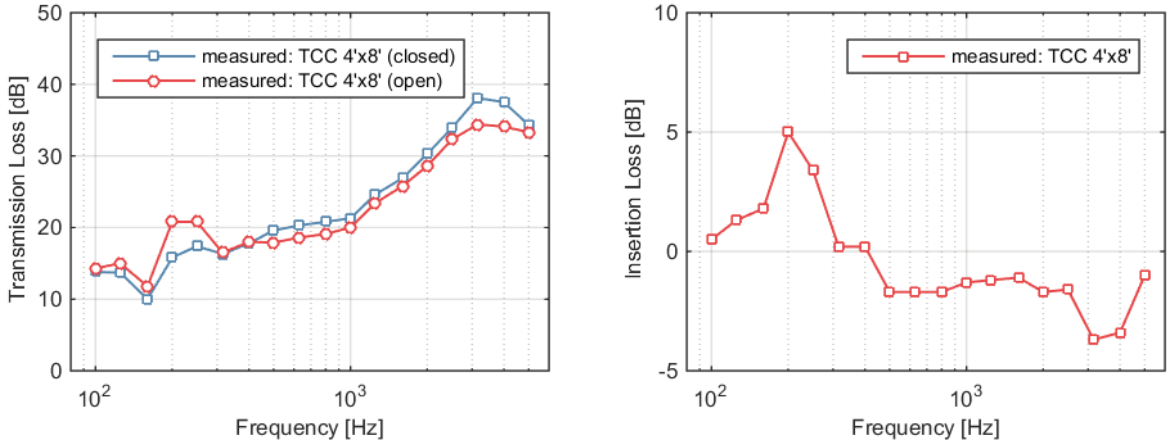

Figure 32: Transmission loss (left) and insertion loss (right) of the 4' by 8' TCC panel with embedded resonators tuned for 200 Hz. Measurements are from tests T15-405 and T15-406.

Figure 33 compares measurements and predictions of insertion loss for the 4' by 4' and 4' by 8' TCC panels. In both cases, the resonators were tuned for 200 Hz. While the maximum insertion loss is similar, the peak is shifted to the right in the measurements collected with the smaller panel. This could be due to vibroacoustic coupling between the acoustic resonators and structural dynamics of the panel, however, the exact cause is not known. Note that the shift is not captured by the models, which yield nearly identical predictions for the two panels. In addition, the model does not capture the negative IL observed above 300 Hz. This is because the model essentially represents the resonators as impedance patches that are superimposed on the structure and does not capture the additional transmission path through the inlets, which becomes significant at high frequencies.

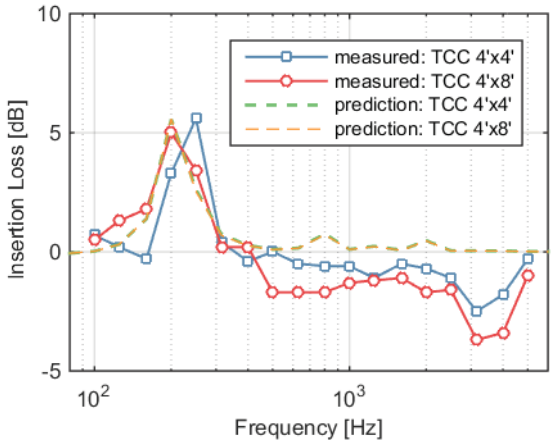

Figure 33: Insertion loss of the 4' by 4' and 4' by 8' TCC panels with embedded resonators tuned for 200 Hz: measurements from tests (T15-401 – T15-400) and (T15-406 – T15-405) (solid lines), and predictions (dashed lines).

Figure 34 compares the performance of TCC panels tuned for different frequencies. Specifically, all of the resonators were tuned for 200 Hz in one case and spread between 200 Hz, 250 Hz, and 315 Hz in the second case. The measured TL is shown in the plot on the left and IL is shown in the plot on the right. First, notice that the green and blue TL curves (on the left) are nearly on top of each other, as is expected for the tests performed with inlets closed (i.e., covered with tape). When the inlets are open, the low frequency TL is improved in both cases. The benefit is shown clearly in the IL plots on the right. Both measurements and predictions show that the

benefit provided by the resonators can be targeted at a single one-third octave band, or spread over multiple bands.

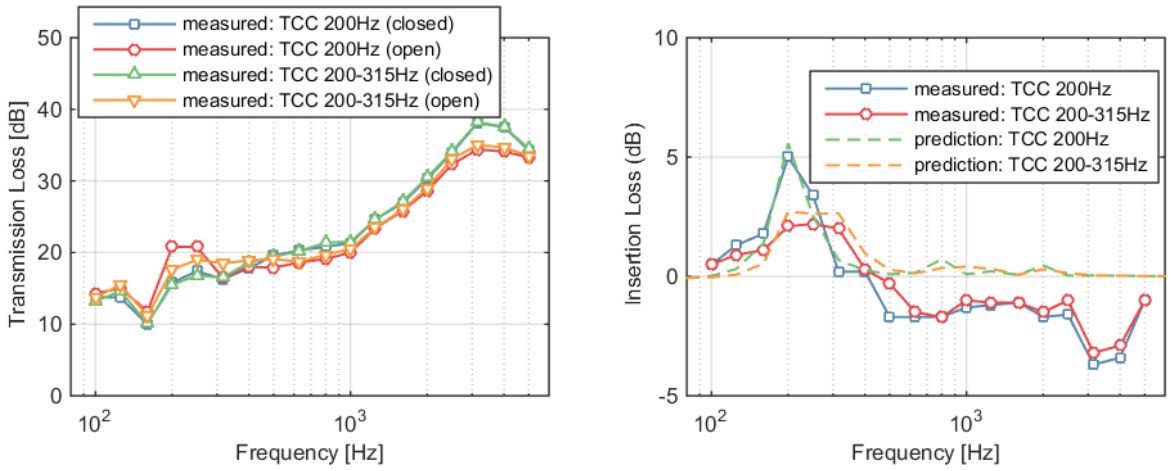

Figure 34: Transmission loss (left) and insertion loss (right) for two different resonator tunings from tests (T15-406 – T15-405) and (T15-404 – T15-403) (solid lines), and predictions (dashed lines).

Combined Configurations

Results from the TL tests with foam over the TCC panel are presented next. Specifically, Figure 35 shows the performance of foam on 2" spacers over the TCC panel. In this case, the resonators were all tuned for 200 Hz. While it is clear that the resonators augment the low-frequency performance around 200 Hz, the foam provides a more broadband benefit that increases with frequency. Therefore, the two types of treatment are complementary. The IL figure on the right shows that the performance of the resonator array and foam are largely independent. In other words, the combined performance is essentially equal to the sum of the IL of each treatment in isolation (as shown by the dashed black line).

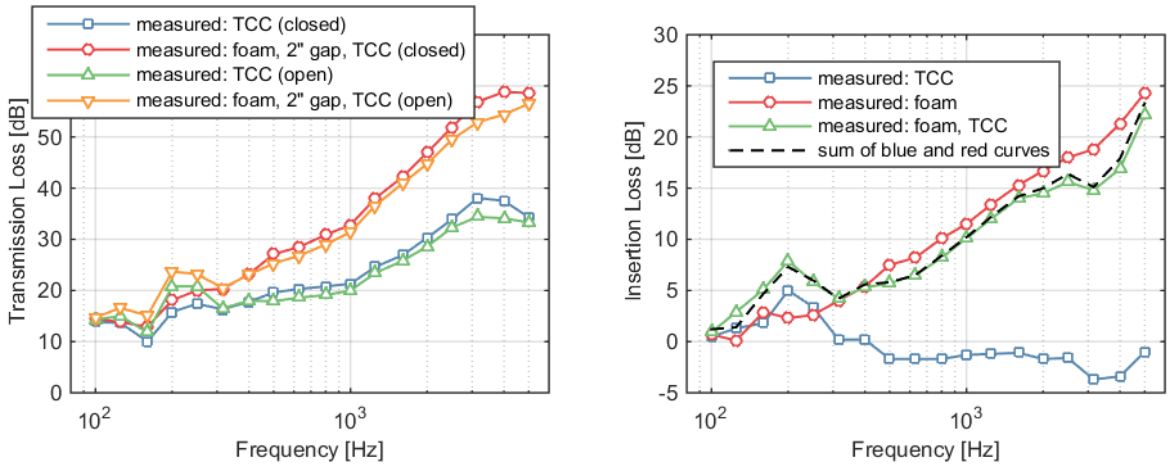

Figure 35: Transmission loss (left) and insertion loss (right) of the TCC panel with foam. Transmission loss measurements from tests T15-405, T15-407, T15-406, and T15-408 (left figure); and insertion loss results (relative to the TCC panel with closed inlets) from tests (T15-406 - T15-405), (T15-407 – T15-405), and (T15-408 – T15-405) (right figure).

Figure 36 shows that the size of the spacers has no effect on TL, at least not for the 1" and 2" spacers used in this study. The predictions shown on the right are consistent with the measurements in this regard. Note that this finding is also consistent with previous work, which found that there was no difference in TL when foam was placed directly against the surface of a panel, or offset from the surface by 1.25" [6].

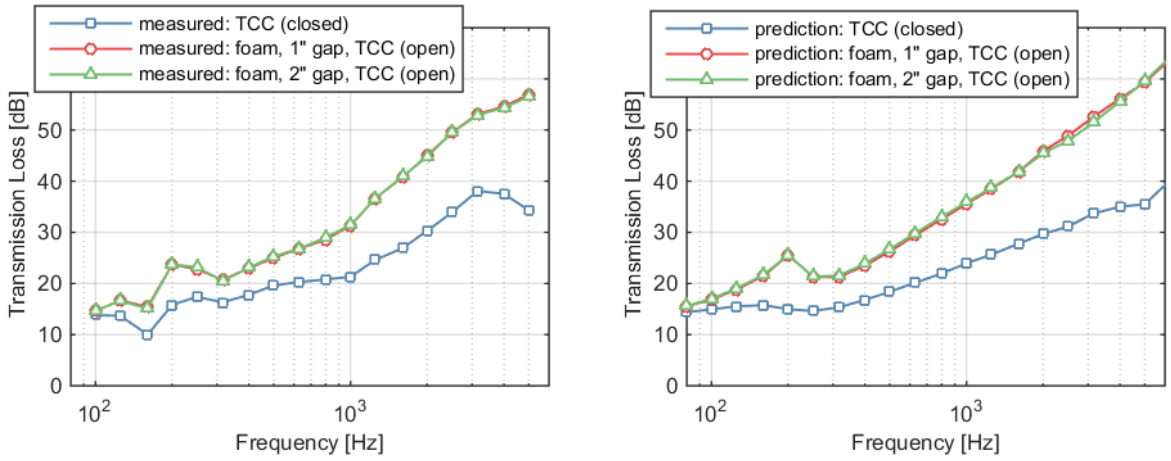

Figure 36: Transmission loss of the TCC panel with foam on spacers: measurements from tests T15-405, T15-411, and T15-408 (left figure); and predictions (right figure).

Figure 37 shows that the coversheet has no effect on the performance of the resonators, but has a small positive impact on TL at high frequencies. Specifically, the coversheet improves the TL by 1-2 dB above 315 Hz. The predictions, shown on the right, also capture this trend.

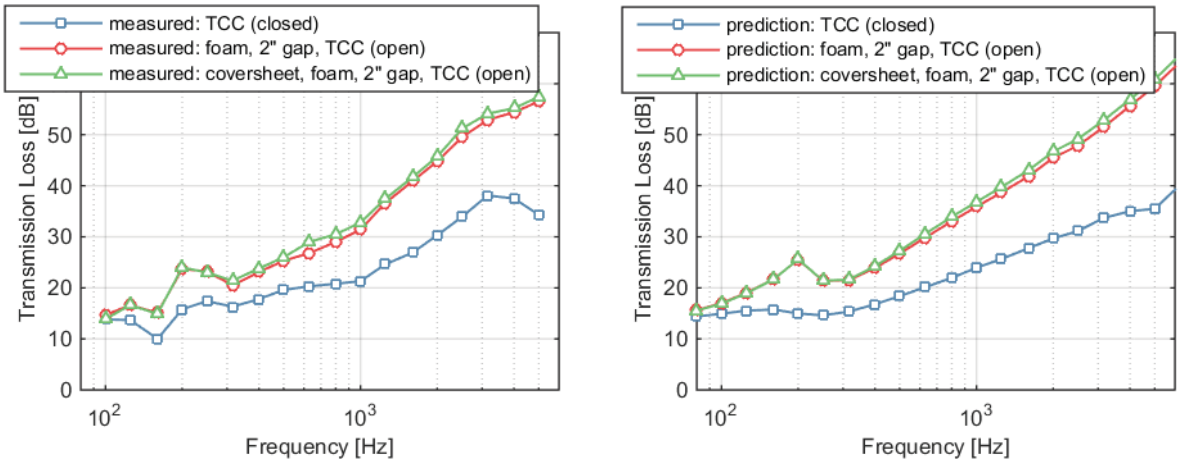

Figure 37: Transmission loss of the TCC panel with foam and a coversheet: measurements from tests T15-405, T15-408 and T15-410 (left figure); and predictions (right figure).

Results from the TL test with foam strips are shown in Figure 38. The foam strips provide some benefit at high frequencies, however, they are not as effective as a full foam slab. As expected, the foam strips have no impact on the performance of the resonators around 200 Hz. Once again, the predictions shown on the right capture the relevant trends.

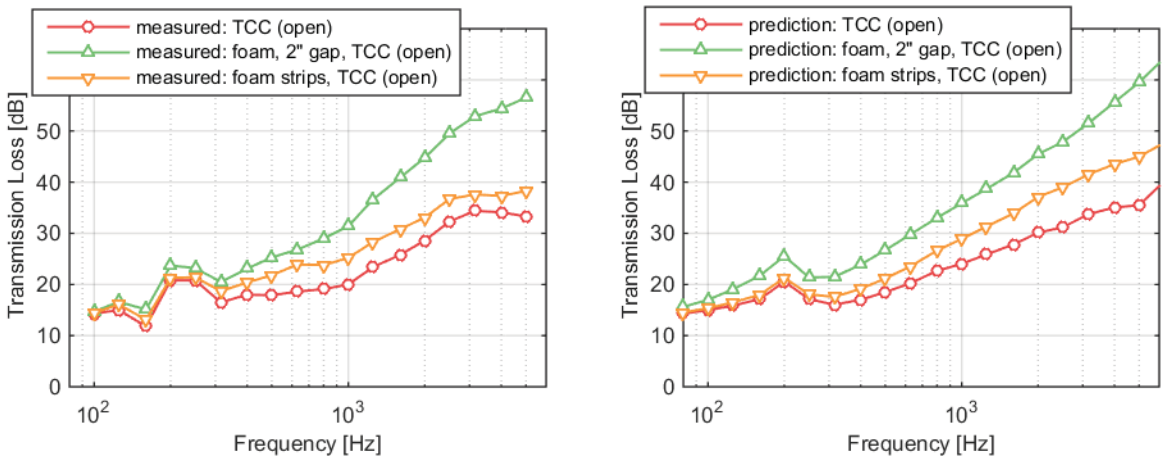

Figure 38: Transmission loss of the TCC panel with foam strips: measurements from tests T15-406, T15-408, and T15-414 (left figure); and predictions (right figure).

Finally, Figure 39 compares the performance of individual treatments (i.e., either foam with a coversheet, or the resonator array) with the combined performance of foam with a coversheet over the TCC panel with open inlets. Specifically, the plot shows the IL, or change in TL relative to the bare TCC panel with closed inlets. Notice the complementary nature of the two technologies. The IL of the foam is relatively small at low frequencies, but increases smoothly with frequency, while the IL of the TCC panel augments the low frequency performance in a narrow frequency range. When used together, the IL of the coversheet, foam and TCC panel is 5 dB or more in all one-third octave bands above 160 Hz. In contrast, when the coversheet and foam are used alone, the IL does not exceed 5 dB until the 315 Hz one-third octave band.

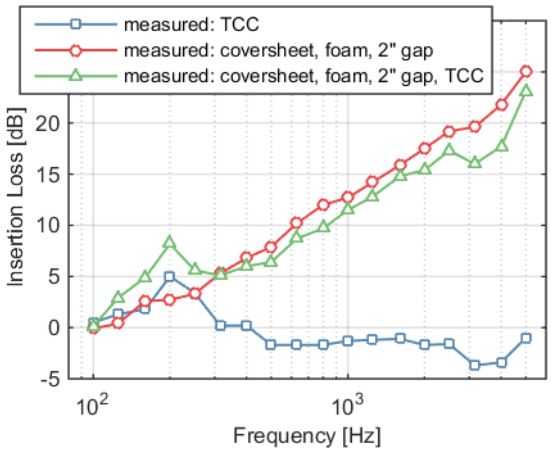

Figure 39: Insertion loss of noise treatments (relative to the TCC panel with closed inlets): measurements from tests (T15-406 - T15-405), (T15-409 – T15-405), and (T15-410 – T15-405).

Concluding Remarks

The results of this test program demonstrate that the tuned chamber core concept is effective when used in isolation or combined with acoustic foam treatments. Specifically, an array of acoustic resonators integrated within the core of the panels was shown to improve both the low-frequency absorption and transmission loss of the structure in targeted one-third octave bands. For instance, with resonators tuned to 200 Hz, the measured Sabine absorption coefficient for the panel with integrated resonators exceeded one, and the transmission loss of the structure was 5 dB larger than it was for the same panel without resonators. When the resonator tunings were

spread over multiple one-third octave bands, the benefit was spread over those same one-third octave bands. These benefits were achieved with no appreciable change in the size or weight of the structure. Results also show that combining acoustic foam with tuned chamber core panels can result in better performance than either technology can provide alone. While the transmission loss benefit is additive, the multi-layer interaction between the resonator array and the foam results in better low-frequency absorption than a simple linear combination would suggest. Furthermore, models are able to capture many of the trends observed in the measurements. The promising results seen during this test series provide further motivation to test larger, and more realistic structures in the future.

References

1. Lane, S. A., Henderson, K., Williams, A., and Ardelean, E., "Chamber Core Structures for Fairing Acoustic Mitigation," *Journal of Spacecraft and Rockets*, Vol. 44, No. 1, 2007.
2. Li, D., and Vipperman, J. S., "Noise Control of Mock-Scale ChamberCore Payload Fairing using Integrated Acoustic Resonators," *Journal of Spacecraft and Rockets*, Vol. 43, No. 4, 2006.
3. Schiller, N. H., Allen, A. R., Zalewski, B. F., and Beck, B. S., "Sound Transmission Loss through a Corrugated-Core Sandwich Panel with Integrated Acoustic Resonators," in *Proceedings of ASME IMECE*, 2014.
4. Allen, A. R., Schiller, N. H., Zalewski, B. F., and Rosenthal, B. N., "Transmission Loss and Absorption of Corrugated Core Sandwich Panels with Embedded Resonators," in *Proceedings of Noise-Con*, 2014.
5. Hughes, W. O., McNelis, A. M., and McNelis, M. E., "Acoustic Test Characterization of Melamine Foam for Usage in NASA's Payload Fairing Acoustic Attenuation System," NASA/TM-2014-218127, 2014.
6. McNelis, A. M., and Hughes W. O., "Acoustic Test Summary of Melamine Foam and other Acoustic Attenuation Concepts in Support of the SLS Fairing Project," NASA Space Launch System (SLS) Spacecraft/Payload Integration and Evolution Office (SPIE) report, 2014.
7. McNelis, A. M., and Hughes, W. O., "Effect of Coversheet Materials on the Acoustic Performance of Melamine Foam," in *Proceedings of the 29th Aerospace Testing Seminar*, 2015.
8. ASTM C423-09a, "Standard Test Method for Sound Absorption and Sound Absorption Coefficients by the Reverberation Room Method," 2009.
9. ASTM E90-09, "Standard Test Method for Laboratory Measurement of Airborne Sound Transmission Loss of Building Partitions and Elements," 2009.
10. Allard, J. F., and Atalla, N., *Propagation of Sound in Porous Media: Modeling Sound Absorbing Materials, Second Edition*, John Wiley & Sons, 2009.
11. Allen, A. R., and Schiller, N. H., "Experimental Evaluation of Equivalent-Fluid Models for Melamine Foam," in *Proceedings of Noise-Con*, 2016.
12. Schiller, N. H., and Allen, A. R., "Assessment of Analytical Predictions for Diffuse Field Sound Transmission Loss," in *Proceedings of InterNoise*, 2015.
13. Miki., Y., "Acoustical Properties of Porous Materials - Modification of Delany-Bazley Models," *Journal of the Acoustical Society of Japan,* Vol. 11, No. 1, 1990.
14. Fahy, F., and Gardonio, P., *Sound and Structural Vibration: Radiation, Transmission, and Response, Second Edition*, Academic Press, 2007.
15. Heckl, M., "Untersuchungen an Orthotropen Platten," *Acta Acustica united with Acustica*, Vol. 10, No. 2, 1960.

16. Allen, A. R., and Schiller, N. H., “Vibroacoustic characterization of corrugated-core and honeycomb-core sandwich panels,” NASA Report, 2016.
17. Narayanan, S., and Shanbhag, R. L., “Sound Transmission through a Damped Sandwich Panel,” *Journal of Sound and Vibration*, Vol. 80, No. 3, 1982.
18. Cummings, A., “Sound Transmission in 180 Degree Duct Bends of Rectangular Section,” *Journal of Sound and Vibration*, Vol. 41, No. 3, 1975.
19. Kinsler, L. E., Frey, A. R., Coppens, A. B., and Sanders, J. V., *Fundamentals of Acoustics, 4th Edition*, John Wiley & Sons, 2000.
20. Schiller, N. H., Allen, A. R., Herlan, J. W., and Rosenthal, B. N., “Experimental Evaluation of Tuned Chamber Core Panels for Payload Fairing Noise Control,” in *Proceedings of the 29th Aerospace Testing Seminar*, 2015.
21. Pritchard R. L., “Mutual Acoustic Impedance between Radiators in an Infinite Rigid Plane,” *Journal of the Acoustical Society of* America, Vol. 32, No. 6, 1960.
22. Brunskog, J., “The Forced Sound Transmission of Finite Single Leaf Walls Using a Variational Technique,” *Journal of the Acoustical Society of America*, Vol. 132, No. 3, 2012.
23. Brouard, B., Lafarge, D., and Allard, J.-F., “A General Method of Modelling Sound Propagation in Layered Media,” *Journal of Sound and Vibration*, Vol. 183, No. 1, 1995.
24. Hughes, W. O., McNelis, A. M., Nottoli, C., and Wolfram, E., “Examination of the Measurement of Absorption using the Reverberant Room Method for Highly Absorption Acoustic Foam,” in *Proceedings of the 29th Aerospace Testing Seminar*, 2015.
25. Swanson, S. R., and Qian, Y., “Multiaxial Characterization of T800/3900-2 Carbon/Epoxy Composites,” *Composites Science and Technology*, Vol. 43, No. 2, 1992.
26. Hexcel Corporation, “HexWeb™ Honeycomb Attributes and Properties,” http://www.hexcel.com/Resources/DataSheets/Brochure-Data-Sheets/Honeycomb_Attributes_and_Properties.pdf, accessed June 2, 2016.
27. Mordecai, Bill: Freudenberg Industrial Nonwovens, Durham, NC, personal communication, 2016.

Appendix A: TCC Panels

The TCC panels are composite sandwich panels with a corrugated core. Three panels with nominally identical construction were built and tested, a 4’ by 8’ panel, and two 4’ by 4’ panels. The panels have a nominal thickness of 2.2”, which includes 0.063”-thick facesheets over a 2.1”-tall corrugated core. The nominal geometry of the core is shown in Figure 40. The facesheets are made with 8 plies of carbon-fiber fabric while the corrugated core consists of 2 fabric plies with a nominal thickness of 0.016”. The layup for the facesheets and core is shown in Table 3. During fabrication, the facesheets and core were pre-cured and then post-bonded with Hysol EA 9394 epoxy paste adhesive.

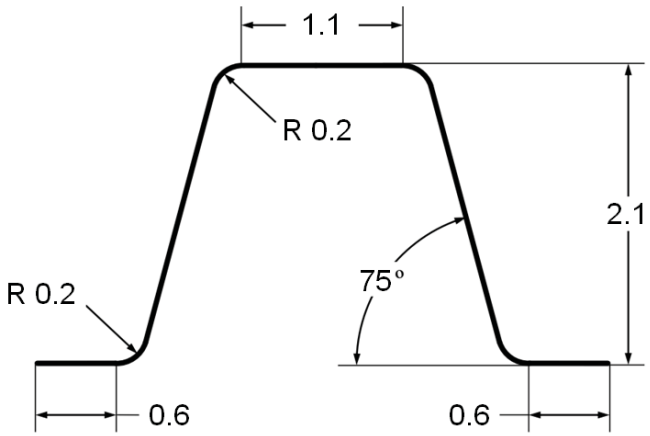

Figure 40: Nominal core geometry for the TCC panels (dimensions are in inches).

Table 3: Layup for the TCC facesheet (left) and corrugated core (right).

Facesheets

Ply Number	Ply Material	Ply Orientation
001	Toray T830H/3900-2D	45/-45
002	Toray T830H/3900-2D	0/90
003	Toray T830H/3900-2D	45/-45
004	Toray T830H/3900-2D	0/90
005	Toray T830H/3900-2D	0/90
006	Toray T830H/3900-2D	45/-45
007	Toray T830H/3900-2D	0/90
008	Toray T830H/3900-2D	45/-45

Corrugated Core

Ply Number	Ply Material	Ply Orientation
001	Toray T830H/3900-2D	45/-45
002	Toray T830H/3900-2D	45/-45

The TCC panels contain 0.875”-diameter holes in the top facesheet, which function as the inlets to the acoustic resonators. The nominal inlet locations for the 4’ by 8’ panel are shown in

Figure 41. The inlet locations for the 4’ by 4’ panels are similar, corresponding to one-half of the 4’ by 8’ panel.

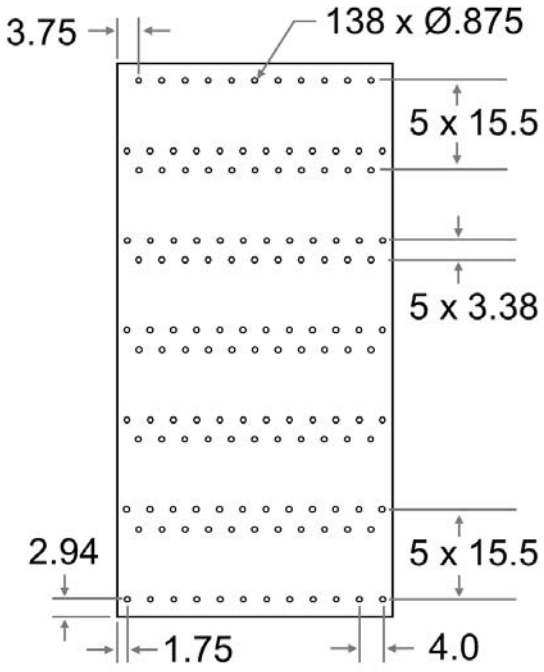

Figure 41: Nominal inlet locations for the 4’ by 8’ TCC panel (dimensions are in inches).

The measured dimensions and mass of the TCC panels were slightly different than the nominal values, and are therefore included in Table 4.

Table 4: Measured parameters for the TCC panels.

	Panel A	**Panels B and C**
Length (in / m)	95.75 / 2.43	48.0 / 1.22
Width (in / m)	47.9 / 1.22	48.0 / 1.22
Overall thickness (in / m)	2.25 / 0.057	2.25 / 0.057
Area Weight (including plugs in the core) (lb/ft^2 / kg/m^2)	1.54 / 7.52	1.61 / 7.86

For the predictions shown in this paper, the TCC panels were approximated as a smeared, orthotropic shell, which is only valid at low frequencies. The formulation requires bending stiffness estimates for both the compliant cross direction and the stiff axial direction. These values were estimated based on a combination of tests and detailed FE models [16]. The apparent wavelengths for the TCC panel are shown in Figure 42 as a function of frequency. The figure also includes dashed lines representing the free flexural wavelengths of an equivalent plate given by

$$\lambda = \frac{2\pi}{(\omega^2 m/D)^{1/4}} \tag{30}$$

where m is the mass per unit area of the panel and D is the bending stiffness (or flexural rigidity). Curves generated using bending stiffness values of 70 lbf-ft and 70x10^3 lbf-ft provide reasonable

agreement with the apparent wavelengths in the cross- and axial-corrugation directions, respectively.

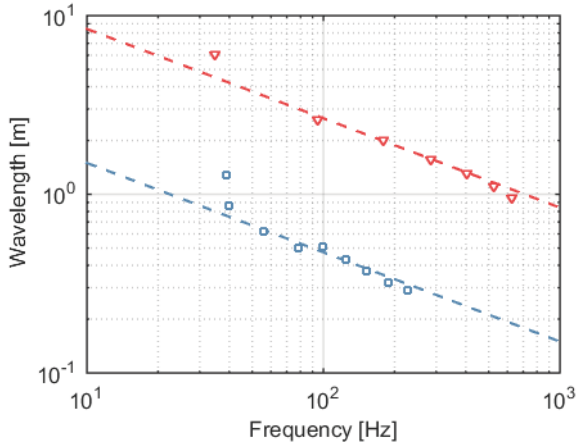

Figure 42: Apparent wavelengths of the TCC panel in the cross-corrugation and axial directions (□,▽). Free flexural wavelengths of an orthotropic plate with bending stiffness D = 70 lb-ft and 70x10³ lb-ft (– –, – –) are also shown.

Appendix B: Honeycomb Panels

The honeycomb panels have a nominal thickness of 1.12”, which includes 0.048”-thick facesheets over a 1”-thick aluminum honeycomb core (Hexcel 3.1 pcf 1/8-5052-.0007). The facesheets are fabricated from 8 plies of uni-directional carbon-fiber epoxy tape (Toray T800/3900-2) with a stacking sequence of $[45,-45,90,0]_S$. The facesheets are bonded to the aluminum core using Cytec FM 300 epoxy film adhesive. The dimensions and mass of the panels (as-built) are included in Table 5. The material properties used to generate the transmission loss predictions for the honeycomb panel are included in Table 6. Specifically, the lamina-elasticity constants for T800/3900-2 were taken from Swanson and Qian [25] and then classical lamination theory (implemented within the Laminate Modeler in MSC Patran) was used to calculate engineering constants for the facesheet laminate. Properties for the core were obtained from Hexcel Corporation [26]. Note that the 1- and 2-directions are in-plane, and the 3-direction is through the thickness. For the core, the 1-direction is the ribbon/L direction.

Table 5: Measured parameters for the honeycomb panels.

	Panel A	Panels B and C
Length (in / m)	95.75 / 2.432	47.75 / 1.213
Width (in / m)	47.75 / 1.213	47.75 / 1.213
Overall thickness (in / m)	1.12 / 0.0284	1.125 / 0.0286
Area Weight (lb/ft^2 / kg/m^2)	1.32 / 6.44	1.39 / 6.79

Table 6: Laminate and core material properties used in the honeycomb sandwich panel model.

	[1]Facesheet Laminate	[2]Core
Material	Toray T800/3900-2	Hexcel 3.1 pcf 1/8-5052-.0007
Layup	$[45/-45/90/0]_S$	-
Thickness (in / m)	0.047 / 1.19×10^{-3}	1.0 / 25.4×10^{-3}
E_1 (psi / Pa)	8.57×10^6 / 5.91×10^{10}	0.094×10^3 / 25×10^6
E_2 (psi / Pa)	8.57×10^6 / 5.91×10^{10}	0.094×10^3 / 25×10^6
E_3 (psi / Pa)	-	75×10^3 / 520×10^6
nu_{12}	0.308	-
G_{13} (psi / Pa)	-	45×10^3 / 310×10^6 (ribbon, L direction)
G_{23} (psi / Pa)	-	22×10^3 / 151×10^6 (warp, W direction)
G_{12} (psi / Pa)	3.28×10^6 / 2.26×10^{10}	1.1×10^3 / 7.6×10^6
rho (lb/ft^3 / kg/m^3)	97.4 / 1560	3.10 / 49.7
[3]Effective density (lb/ft^3 / kg/m^3)	132 / 2120	4.21 / 67.5

[1]Laminate properties calculated using classical lamination theory with lamina properties from Swanson and Qian [25]
[2]Core properties from Hexcel datasheet [26]
[3]Accounts for the mass of the adhesive film

Appendix C: Foam and Coversheet Properties

Ultra-light melamine foam from Soundcoat was used in this test series. The foam was 4” thick and included, in some cases, a porous, non-woven fabric coversheet called SoundTex. Nominal properties for the foam and coversheet are given in Table 7.

Table 7: Foam and coversheet properties.

	Soundfoam ML ULb foam	SoundTex coversheet
Thickness (in / m)	4.0 / 0.10	0.011 / 2.7×10^{-4}
Density (lb/ft^3 / kg/m^3)	0.37 / 6.0	-
Mass per unit area (lb/ft^2 / kg/m^2)	-	0.012 / 0.059
[1]Specific Flow Resistance ($lbf\text{-}s/ft^3$ / Ns/m^3)	-	1.2 / 190
[2]Flow resistivity ($lbf\text{-}s/ft^4$ / Ns/m^4)	18 / 9400	-

[1]personal communication [27]
[2]based on raylometer measurements of ML ULb documented by Allen and Schiller [11]

REPORT DOCUMENTATION PAGE

Form Approved
OMB No. 0704-0188

1. REPORT DATE *(DD-MM-YYYY)*
01- 09 - 2016

2. REPORT TYPE
Technical Memorandum

3. DATES COVERED *(From - To)*

4. TITLE AND SUBTITLE
Tuned Chamber Core Panel Acoustic Test Results

5a. CONTRACT NUMBER

5b. GRANT NUMBER

5c. PROGRAM ELEMENT NUMBER

6. AUTHOR(S)
Schiller, Noah H.; Allen, Albert R.

5d. PROJECT NUMBER

5e. TASK NUMBER

5f. WORK UNIT NUMBER
585777.08.50.66.23.10

7. PERFORMING ORGANIZATION NAME(S) AND ADDRESS(ES)
NASA Langley Research Center
Hampton, VA 23681-2199

8. PERFORMING ORGANIZATION REPORT NUMBER
L-20748

9. SPONSORING/MONITORING AGENCY NAME(S) AND ADDRESS(ES)
National Aeronautics and Space Administration
Washington, DC 20546-0001

10. SPONSOR/MONITOR'S ACRONYM(S)
NASA

11. SPONSOR/MONITOR'S REPORT NUMBER(S)
NASA-TM-2016-219338

12. DISTRIBUTION/AVAILABILITY STATEMENT
Unclassified - Unlimited
Subject Category 71
Availability: NASA STI Program (757) 864-9658

13. SUPPLEMENTARY NOTES

14. ABSTRACT
This report documents acoustic testing of tuned chamber core panels, which can be used to supplement the low-frequency performance of conventional acoustic treatment. The tuned chamber core concept incorporates low-frequency noise control directly within the primary structure and is applicable to sandwich constructions with a directional core, including corrugated-, truss-, and fluted-core designs. These types of sandwich structures have long, hollow channels (or chambers) in the core. By adding small holes through one of the facesheets, the hollow chambers can be utilized as an array of low-frequency acoustic resonators. These resonators can then be used to attenuate low-frequency noise (below 400 Hz) inside a vehicle compartment without increasing the weight or size of the structure. The results of this test program demonstrate that the tuned chamber core concept is effective when used in isolation or combined with acoustic foam treatments. Specifically, an array of acoustic resonators integrated within the core of the panels was shown to improve both the low-frequency absorption and transmission loss of the structure in targeted one-third octave bands.

15. SUBJECT TERMS
Absorption; Chamber; Core; Loss; Sound; Transmission; Tuned

16. SECURITY CLASSIFICATION OF:			17. LIMITATION OF ABSTRACT	18. NUMBER OF PAGES	19a. NAME OF RESPONSIBLE PERSON
a. REPORT	b. ABSTRACT	c. THIS PAGE			STI Help Desk (email: help@sti.nasa.gov)
U	U	U	UU	44	19b. TELEPHONE NUMBER *(Include area code)* (757) 864-9658